Modification of Long Equatorial Rossby Wave Phase Speeds by Zonal Currents

Theodore S. Durland *

Dudley B. Chelton

Roland A. de Szoeke

Roger M. Samelson

College of Oceanic and Atmospheric Sciences

Oregon State University, Corvallis

* *Corresponding author address:* Theodore S. Durland, College of Oceanic and Atmospheric Sciences, Oregon State University, Corvallis, OR 97331.

E-mail: tdurland@coas.oregonstate.edu

ABSTRACT

Previously un-addressed aspects of equatorial currents' effects on long-Rossby-wave phase speeds are investigated using solutions of the shallow-water equations linearized about semi-realistic currents. Modification of the background potential vorticity (pv) gradient by curvature in the narrow equatorial currents is shown to play a role comparable to the Doppler shift emphasized by previous authors. The important variables are shown to be the meridional projections of mean-current features onto relevant aspects of the wave field. Doppler shifting of long Rossby waves is determined by the projection of the mean currents onto the wave's squared zonal-velocity and pressure fields. Pv-gradient modification matters only to the extent that it projects onto the wave field's squared meridional velocity.

Because the zeros of an equatorial wave's meridional velocity are staggered relative to those of the zonal velocity and pressure, and because the meridional scales of the equatorial currents are similar to those of the low-mode Rossby waves, different parts of the current system dominate the advective and pv-gradient modification effects on a single mode. Because the equatorial symmetry of classical equatorial waves flip-flops with increasing meridional mode number, the currents produce opposite effects on adjacent modes. Meridional mode 1 is slowed primarily by a combination of eastward advection by the Equatorial Undercurrent (EUC) and the pv-gradient decrease at the peaks of the South Equatorial Current (SEC). The mode-2 phase speed, in contrast, is increased primarily by a combination of westward advection by the SEC and the pv-gradient increase at the core of the EUC.

1. Introduction

The classical theory of equatorial waves in a rest-state ocean is well developed (Matsuno, 1966; Moore and Philander, 1977), but the strong zonal currents typical of the equatorial oceans are known to affect both the meridional structures and the dispersion relations of these waves. A number of studies have sought to characterize and explain these effects and they are summarized nicely by McPhaden and Ripa, 1990. Three theoretical works in particular have illuminated the influence of mean equatorial currents on stable long Rossby waves, our primary concern in this paper. Philander, 1979, analyzed the effect of an equatorially-symmetric eastward jet (mimicking the Equatorial Undercurrent) on the lowest meridional mode of a single baroclinic mode. While noting the mismatch between the vertical scales of the baroclinic modes and that of the Equatorial Undercurrent, he demonstrated that valuable information about the real ocean could nevertheless be deduced from this approach. Philander, 1979, showed that the westward phase speed of the meridional-mode-1 Rossby wave was slowed and the peaks in the pressure eigenfunction were shifted poleward by the presence of his idealized undercurrent.

Ripa and Marinone, 1983, solved a perturbation problem for $1^1/_2$-layer linearized waves in the presence of an equatorially-symmetric zonal jet with either eastward or westward velocity. They showed the modified eigenfunctions for the meridional-mode-2 long Rossby wave and the modified dispersion relations for the lowest four meridional-mode Rossby waves. The westward phase speeds of modes 1, 3 and 4 were shown to be faster in the presence of the westward jet than in the presence of the eastward jet, in accordance with the expected Doppler effect. It was less clear whether either jet had any effect on the mode 2 phase speed in the long-Rossby wave range. Besides the Doppler shift, Ripa and Marinone, 1983, demonstrated the effect of the background layer-thickness deviations on the speed of inertia-gravity waves. They did not, however, address any additional phase-speed altering mechanisms in the case of long Rossby waves. An important point that their analysis brought out was that

the Doppler shift and the effect of varying background layer thickness depend not just on the magnitude of the background fields but on how these project onto the appropriate eigenfunctions - a point that will play a prominent role in our analysis. The mode-2 Rossby-wave eigenfunction peaks in the solutions of Ripa and Marinone, 1983, were shifted equatorward in the presence of the westward jet and poleward in the presence of the eastward jet, in agreement with the mode-1 distortion found by Philander, 1979.

Proehl, 1990, included both the meridional and vertical structure of the equatorial currents in his study of their influence on meridional-mode-1 long Rossby waves via WKB solutions, a perturbation expansion and direct numerical integrations. Using an equatorially symmetric, but otherwise realistic profile of the Equatorial Undercurrent and overlying South Equatorial Current, he solved the linearized equations to determine the effects on the lowest few vertical modes. While distortions of the higher vertical modes were significant, the near-surface changes to the first baroclinic mode were quite similar to those produced by the single-layer calculations of Philander, 1979. The main effect on the pressure eigenfunction was the poleward migration of the peaks above the undercurrent and a decrease in the signal below.

In his perturbation solution, Proehl, 1990, noted that the Doppler shift is determined by the projection of the mean current onto the squared eigenfunction of zonal velocity or pressure. He also described an additional phase-speed-altering mechanism as "the projection of the advection of background momentum and density fields by the meridional circulation of the $O(\epsilon)$ wave field (v_0, w_0), upon the wave structures." We will see that this is a reasonable qualitative description of the solution's mathematical form, but it does not provide a useful physical insight into the phase speed modification.

Surprisingly, none of the above-mentioned papers (including the review by McPhaden and Ripa, 1990) addressed the impact of the mean current on the background potential vorticity (pv) gradient, although this effect is known to be important in the phase-speed modification of mid-latitude Rossby waves. Chang and Philander, 1989, used a semi-geostrophic, $1^1/_2$-

layer model to analyze mid-latitude Rossby-wave rays propagating toward the equatorial zone. They noted that their formulation was not valid in the immediate vicinity of the equator (within 2–3 degrees of latitude), but their analysis showed the local importance at low latitudes of an "effective beta" and an "effective radius of deformation", each of which is modified from the rest-state equivalent by shear in the background current and changes in the background layer thickness. Zheng et al., 1994, included the mean-current curvature in a quasi-geostrophic model in an attempt to predict the phase speeds of near-equatorial Rossby waves. Although neither of the above formulations can be used directly to infer the changes in modes that span the equator, the results of Chang and Philander, 1989, provide an impetus for revisiting the analyses of Ripa and Marinone, 1983, and Proehl, 1990, with an eye toward extracting more physical insight into the phase-speed modifying mechanisms of the equatorial current system.

Chelton et al., 2003, (hereafter C03) numerically solved the $1^1/_2$-layer equations linearized about realistic equatorial currents to determine the mean-flow-modified eigenfunctions and dispersion relation for the first-meridional-mode, annual long Rossby wave; equivalent to the approach of Philander, 1979, but with more realistic current profiles. This was done at numerous longitudinal locations across the Pacific, using upper-layer currents obtained by averaging the mean-zonal-current ADCP transects of Johnson et al., 2002, over the upper 250 meters. The vertically-averaged current systems contain recognizable representations of the eastward flowing Equatorial Undercurrent (EUC) and North Equatorial Countercurrent (NECC), and of the southern (SECS) and northern (SECN) branches of the westward flowing South Equatorial Current (SEC).

While acknowledging the shortcomings of the $1^1/_2$-layer approach, C03 showed that the theoretical pressure eigenfunctions thus derived bear a strong resemblance to the altimetrically observed quasi-annual sea surface height (SSH) anomalies over most of the east-central equatorial Pacific. In their solutions, the mean-current modifications at $140W$ include a slowing of the phase speed by about 15% and a distortion of the classical, twin-peaked pres-

sure eigenfunction (symmetric about the equator) such that the amplitude of the distorted wave's northern extremum is roughly twice that of the southern extremum. The mean currents and wave modifications at $140W$ were found to be typical of the equatorial Pacific between $155W$ and $110W$.

The goal of this paper is to illuminate the physical mechanisms by which the equatorial current system alters the phase speeds of long Rossby waves. We will focus on the effects of semi-realistic, equatorial-Pacific currents on the lowest two meridional modes in a $1^1/_2$-layer format. Higher modes are stable in the $1^1/_2$-layer model, but their slower phase speeds are probably exceeded by parts of the SEC in its full vertical profile, so that critical surfaces and wave absorption are likely in the real ocean. The modified phase speeds of modes 1 and 2, however, appear fast enough that these modes can exist as stable waves. Two meridional profiles of zonal currents will be utilized, based on C03's upper-layer currents at $140W$ and $170W$. The former represent the most robust mean currents found in the equatorial oceans and the latter represent a transition zone between the central Pacific currents and the weaker currents of the western Pacific. As noted by C03, the effect of the latter currents on the long Rossby waves is qualitatively different than the effect of the former.

The first interesting result of our investigation is that the second meridional mode can be modified in a way that appears to be exactly opposite to the modifications of mode 1. In contrast to the effects on mode 1 described above (and in C03), we show here that the $140W$ currents *increase* the phase speed of mode 2 and distort its SSH structure (antisymmetric in the classical solution) so that the *southern* extremum is roughly twice as large as the northern one. At $170W$, the mean currents do not produce a significant asymmetry in the eigenfunctions of mode 2 (similarly to C03's results for mode 1) but the effect on the dispersion relations of the two modes is still quite different. While mode 1 is slowed significantly at $170W$, the phase speed of mode 2 is hardly changed.

Clearly, the effect of the currents on the Rossby waves can not be encapsulated in a single, catch-all description, and the bulk of this paper is dedicated to developing a formalism by

which we can analyze the effects of the current-system components on long Rossby waves. We then use the analysis to explain the reasons for the above-noted differences in the effects of different current systems on a single mode and of a single current system on different modes.

Our approach is a perturbation-expansion formulation similar to those of McPhaden and Knox, 1979, Ripa and Marinone, 1983, and Proehl, 1990, but most closely following the formalism of the second of these studies. The wave currents are small compared to the mean currents and the Rossby number of the mean currents is also small, so that the solutions are perturbations on the classical Hermite-function solutions for an equatorial β-plane basin with no mean flow. The differences between our approach and that of Ripa and Marinone, 1983, are several. First, they examined the effect of a single, Gaussian jet while we use the semi-realistic current systems of C03. Second, we extend our linearized analysis to second order in the perturbation parameter, which provides important insights that are not available with only the lower order solution. Finally, we recast the mathematical expressions for the perturbation corrections to reflect the expected physical mechanisms by which the mean currents affect Rossby-wave speeds: advection, modification of the background pv gradient, and modification of the local deformation radius. The various expressions are then evaluated numerically and analyzed graphically for an enhanced understanding of the dynamics that contribute to the wave-speed modifications.

Most of our solutions are calculated at the annual period, but they are representative of the entire long-Rossby wave domain for both meridional modes, i.e. all wave periods intraseasonal ($\approx$ 60 days) or longer. The only noticeable change throughout this range is the ratio between the meridional wave-velocity amplitude and that of the zonal wave velocity; a ratio that decreases with increasing period. We do not consider zonal and temporal variability in the background currents, and the $1^1/_2$-layer approach naturally ignores the effects of vertical shear on the waves. Given our incomplete knowledge of the zonal current effects, however, our analysis provides an important next step in the improvement of our understanding.

Section 2 presents the nondimensional equations with which we will work and the background current profiles at $140W$ and $170W$ which will be used in our analysis. In addition, numerical eigenvalue solutions for modes 1 and 2 in the two different current systems will be shown in order to set up the specific questions we wish to answer with the perturbation analysis. The perturbation problem is developed in section 3 and we present the solutions in section 4. Section 5 contains an analysis of how the various aspects of the mean current system contribute to dispersion-relation modifications, and section 6 summarizes our results.

2. Numerical Solutions

a. Equations

Our mathematical framework is the non-dimensional shallow water equations on the equatorial β-plane:

$$\partial_t \tilde{\underline{u}} + \tilde{\underline{u}} \cdot \nabla \tilde{\underline{u}} + y\, \hat{\underline{k}} \times \tilde{\underline{u}} + \nabla \tilde{\eta} = 0, \tag{1}$$

$$\partial_t \tilde{\eta} + \nabla \cdot [(1 + \tilde{\eta}) \tilde{\underline{u}}] = 0, \tag{2}$$

which represent the dynamics of a $1^1/_2$-layer model with mean layer thickness H_0 and reduced gravity g'. The layer thickness deviation, $\tilde{\eta}$, is normalized by H_0 while the vector velocity, $\tilde{\underline{u}}$ (with zonal and meridional components $\tilde{u}$ and $\tilde{v}$), is normalized by the Kelvin wave speed, $c = \sqrt{g' H_0}$. Zonal and meridional distances, x and y, are normalized by the equatorial deformation radius, $L_e = \sqrt{c/\beta}$, and time, t, is normalized by the equatorial time scale, $T_e = 1/\sqrt{\beta c}$, where β is the Coriolis parameter's meridional derivative at the equator. We will assume an equatorial deformation radius of 340 km. (3.1° latitude), which corresponds to a Kelvin wave speed of 2.7 m/s; typical of the first baroclinic mode in the central equatorial Pacific (Chelton et al., 1998). The corresponding time scale is 1.5 days.

Consider a small amplitude wave field superimposed on a zonal current system that is

independent of x and t:

$$\begin{pmatrix} \tilde{u} \\ \tilde{v} \\ \tilde{\eta} \end{pmatrix} = \begin{pmatrix} U(y) \\ 0 \\ \delta H(y) \end{pmatrix} + \epsilon \begin{pmatrix} \hat{u}(x,y,t) \\ \hat{v}(x,y,t) \\ \hat{\eta}(x,y,t) \end{pmatrix}, \tag{3}$$

where $\epsilon \ll 1$ and the variable terms on the right-hand-side (rhs) are $O(1)$. At lowest order the flow is geostrophic:

$$y\,U + \delta H' = 0, \tag{4}$$

where the prime indicates a derivative with respect to y. H_0 is chosen so that the average of $\delta H(y)$ vanishes over the range $|y| < 3$ (roughly $\pm 9^\circ$ latitude).

At $O(\epsilon)$ we have the familiar shallow-water equations linearized about U and δH. After a Fourier transform in x and t, these are

$$-i\sigma u + ikUu + (U' - y)v + ik\eta = 0, \tag{5}$$

$$-i\sigma v + ikUv + yu + \eta' = 0, \tag{6}$$

$$-i\sigma\eta + ikU\eta + (1+\delta H)iku + [(1+\delta H)v]' = 0, \tag{7}$$

where

$$(\hat{u}\ \hat{v}\ \hat{\eta}) = \int\int [u(y)\ v(y)\ \eta(y)]\, e^{i(kx-\sigma t)}\, dk\, d\sigma. \tag{8}$$

The zonal wavenumber (k) and frequency (σ) have been non-dimensionalized by L_e^{-1} and T_e^{-1}, respectively.

Equations (5)-(7) are discretized on a staggered grid, with all dependent variables constrained to vanish at $\pm 20^\circ$ latitude. The matrix eigenvalue problem is then solved numerically, with k fixed and σ being the eigenvalue.

b. Background Currents

The mean upper-layer current structures that we will use, along with the corresponding mean layer-thickness deviations, are displayed in fig. 1. They are smoothed and tapered

versions of the currents used by C03 for $140W$ (upper panel) and $170W$ (lower panel). The structure at $140W$ is typical of the equatorial Pacific mean currents from $155W$ to $110W$, and it is in this span where distortions of the rest-state eigensolutions by the mean-flow effects are maximal. We include consideration of the $170W$ currents because the distortions of the eigensolutions are quite different at this longitude in spite of the SECS, EUC and NECC magnitudes being of the same order as at $140W$. As noted by C03, the biggest difference between the two profiles is the absence of an SECN at $170W$.

c. Dispersion Relations

The dispersion curves for both the classical, rest-state solutions and those modified by the two current systems can be seen in fig. 2. As noted, mode-1 long waves are slowed by both current systems, while mode-2 long wave speeds are increased at $140W$ and barely affected at $170W$. In addition to highlighting the specific physical mechanisms involved, our perturbation analysis will be intended to answer the obvious questions posed by this figure: why does a single current system affect the two adjacent modes so differently and why do the two mostly similar current systems affect a single mode so differently?

d. Eigenfunctions

Although our primary focus in this paper is not the eigenfunction distortions, we will see that they play a role in the dispersion-relation modifications and it is worthwhile to understand the qualitative nature of the distortions. The numerical eigenfunction solutions also provide a benchmark against which we can judge the adequacy of the perturbation solutions.

The rest-state and $140W$-distorted eigenfunctions at the annual period appear in fig. 3. Note that v is an order of magnitude smaller than u and η. While the ratio of $|u|_{max}$ to $|v|_{max}$ increases with increasing wave period, the relative structures seen in fig. 3 remain virtually

unchanged for all periods intraseasonal and longer. The previously discussed asymmetry in mode 1's η structure at 140W is clearly seen , with the northern peak having roughly twice the amplitude of the southern peak. The asymmetry introduced in the η eigenfunction of mode 2 is complementary to that of mode 1: the southern peak has roughly twice the amplitude of the northern peak. The peaks in the mode-1 η structures at $140W$ are shifted poleward from the classical solutions by 1-2° of latitude, as noted by C03. This is also true of the northern peak of mode 2, but the southern peak is shifted slightly equatorward.

Figure 4 shows the rest-state and mean-current-modified eigenfunctions at $170W$ in the same format as fig. 3. The striking asymmetries are not produced at this longitude, with the most noticeable changes in the η eigenfunctions being the poleward shifts of the peaks and the widening of mode 1's northern peak.

3. Perturbation Expansion

We seek to understand the current-modified solutions as perturbations on the familiar no-mean-flow solutions, so we will now consider an $O(\epsilon)$ mean current system:

$$\begin{pmatrix} \tilde{u} \\ \tilde{v} \\ \tilde{\eta} \end{pmatrix} = \epsilon \begin{pmatrix} \widehat{U}(y) \\ 0 \\ \widehat{\delta H}(y) \end{pmatrix} + \epsilon^3 \begin{pmatrix} \hat{u}(x,y,t) \\ \hat{v}(x,y,t) \\ \hat{\eta}(x,y,t) \end{pmatrix}. \tag{9}$$

The hatted variables on the rhs of (9) have been rendered $O(1)$ through normalization by the appropriate power of the perturbation parameter, $\epsilon \ll 1$. The latter is a measure of the background-current amplitude normalized by the gravity-wave speed, which can be interpreted as the equatorial Rossby number of the mean current. Inspection of fig. 1 suggests that in our full-strength current scenarios we will be dealing with a value of ϵ that is $O(10^{-1})$.

The ϵ^2 scale separation between the background currents and wave fields is in part a mathematical convenience that simplifies the formulation by avoiding double perturbation parameters. We will formulate a linear eigenvalue problem, so linking the wave field ampli-

tude to the mean current's Rossby number places no actual restriction on the eigenfunction amplitudes other than the upper limit of ϵ^2. The particular choice of scale separation will allow us to carry our linearized perturbation solution to $O(\epsilon^2)$.

Substituting (9) into (1)-(2), the lowest order solution is again the geostrophic balance of the background current (see 4). With this constraint the equations can be written

$$\left[\begin{pmatrix} \partial_t & -y & \partial_x \\ y & \partial_t & \partial_y \\ \partial_x & \partial_y & \partial_t \end{pmatrix} + \epsilon \begin{pmatrix} \widehat{U}\partial_x & \widehat{U}' & 0 \\ 0 & \widehat{U}\partial_x & 0 \\ \widehat{\delta H}\partial_x & (\widehat{\delta H}' + \widehat{\delta H}\partial_y) & \widehat{U}\partial_x \end{pmatrix} + O(\epsilon^3)\right] \begin{pmatrix} \hat{u} \\ \hat{v} \\ \hat{\eta} \end{pmatrix} = 0, \qquad (10)$$

where the $O(\epsilon^3)$ terms are the nonlinear wave-wave interactions.

We limit ourselves to $O(\epsilon^2)$ accuracy and again perform a Fourier transform as in (8). Equation (10) becomes a linear eigenvalue problem with the mean-current effects appearing at $O(\epsilon)$:

$$(\mathcal{L}_k + \epsilon\,\mathcal{N}_k - i\sigma)\,[u(y)\; v(y)\; \eta(y)]^T = 0, \qquad (11)$$

with boundedness conditions on $-\infty < y < \infty$. The operator $(\mathcal{L}_k - i\sigma)$ is the linear shallow-water operator, and $\mathcal{N}_k$ represents the linearized effects of the mean current:

$$(\mathcal{L}_k - i\sigma) = \begin{pmatrix} -i\sigma & -y & ik \\ y & -i\sigma & \frac{d}{dy} \\ ik & \frac{d}{dy} & -i\sigma \end{pmatrix}, \qquad \mathcal{N}_k = \begin{pmatrix} ik\widehat{U} & \widehat{U}' & 0 \\ 0 & ik\widehat{U} & 0 \\ ik\widehat{\delta H} & (\widehat{\delta H}' + \widehat{\delta H}\frac{d}{dy}) & ik\widehat{U} \end{pmatrix}. \qquad (12)$$

Both σ and the wave vector are expanded in powers of ϵ:

$$\sigma = \sum_p \sigma_p \epsilon^p, \qquad (u\; v\; \eta) = \sum_p (u_p\; v_p\; \eta_p)\epsilon^p, \qquad (13)$$

with the linearized approximation valid up to $p{=}2$. At $O(1)$ we have the rest-state equation:

$$(\mathcal{L}_k - i\sigma_0)\,(u_0\; v_0\; \eta_0)^T = 0. \qquad (14)$$

At the higher orders:

$$(\mathcal{L}_k - i\sigma_0) \begin{pmatrix} u_p \\ v_p \\ \eta_p \end{pmatrix} + \mathcal{N}_k \begin{pmatrix} u_{p-1} \\ v_{p-1} \\ \eta_{p-1} \end{pmatrix} - i\sum_{q=1}^{p} \sigma_q \begin{pmatrix} u_{p-q} \\ v_{p-q} \\ \eta_{p-q} \end{pmatrix} = 0, \qquad p = 1, 2. \qquad (15)$$

The separate orders of the perturbation-expansion solutions are identified with single subscripts, while the eigenvalues and eigenfunctions of (14) will be labeled with double subscripts:

$$\sigma_{mn}, \quad (u_{mn}\, v_{mn}\, \eta_{mn}), \quad m = -1, 0, 1, 2, \cdots; \quad n = 1, 2, 3. \tag{16}$$

These are the classical solutions based on Hermite functions (Moore and Philander, 1977), with the first subscript, m, indicating the meridional mode number. For $m \geq 1$, a single zonal wavenumber is associated with three solutions to the frequency equation, representing the inertia-gravity wave with eastward phase propagation ($n=1$), the Rossby wave ($n=2$) and the inertia-gravity wave with westward phase propagation ($n=3$). For $m=0$, the unbounded plane admits only the Yanai (or mixed Rossby-gravity) wave solution with eastward ($n=1$) or westward ($n=3$) phase propagation. The eastward propagating Kelvin wave is identified by $m=-1$, $n=1$, and is the only wave type associated with this value of m. The $m=-1$, $n=2,3$ vectors and the $m=0$, $n=2$ vector are identically zero, and the combination of all the above modes and wave types forms a complete, orthogonal basis from which an arbitrary wave-vector, $(u\, v\, \eta)$, can be constructed (Ripa, 1982). The non-zero eigenvectors are normalized so that

$$\int_{-\infty}^{\infty} dy\, |u_{mn}|^2 + |v_{mn}|^2 + |\eta_{mn}|^2 = 1. \tag{17}$$

We emphasize some important properties of the Hermite-solution wave vectors. First, the zonal velocity and pressure, u_{mn} and η_{mn}, are 90° out of phase with the meridional velocity, v_{mn}. We follow the usual convention and consider v_{mn} to be real while u_{mn} and η_{mn} are imaginary. Second, for $m \geq 0$, v_{mn} is either symmetric or anti-symmetric about the equator, and both u_{mn} and η_{mn} have the opposite symmetry to v_{mn} (note that $v_{-1,1} \equiv 0$). Thus, the wave vector $(u_{mn}\ v_{mn}\ \eta_{mn})$ can be assigned a single symmetry, with the relative symmetries of the individual components implied, and we will use the symmetry of η_{mn} to label the symmetry of the wave vector. Third, the symmetry of these classical wave vectors alternates with increasing meridional mode number: η_{mn} is symmetric about the equator when m is odd, and antisymmetric about the equator when m is even.

The $O(1)$ solution is equated to a single Hermite eigenmode of unit amplitude:

$$\sigma_0 = \sigma_{MN}, \qquad (u_0\ v_0\ \eta_0) = (u_{MN}\ v_{MN}\ \eta_{MN})\,, \tag{18}$$

where M and N are specific values of m and n identifying the particular wave under consideration. The $O(\epsilon^p)$ wave-vector corrections are now expanded in the eigenvectors of (14):

$$(u_p\ v_p\ \eta_p) = \sum_{m,n} A^p_{mn}\,(u_{mn}\ v_{mn}\ \eta_{mn})\,, \qquad p = 1, 2. \tag{19}$$

The linearity of (13) allows us to absorb all contributions of mode $_{MN}$ into the $O(1)$ part so that $A^1_{MN} = A^2_{MN} = 0$, and the linearity of (11) allows us to scale the solution so that the coefficient of $(u_{MN}\ v_{MN}\ \eta_{MN})$ in (18) is one.

Employing the expansion (19) in (15), multiplying on the left by $(u_{st}\ v_{st}\ \eta_{st})^*$ (complex conjugate) and integrating over the domain, we have at $O(\epsilon)$

$$\sigma_1 = -i \int_{-\infty}^{\infty} (u_{MN}\, v_{MN}\, \eta_{MN})^*\, \mathcal{N}_k \begin{pmatrix} u_{MN} \\ v_{MN} \\ \eta_{MN} \end{pmatrix} dy, \tag{20}$$

$$A^1_{st} = \frac{i}{\sigma_{st} - \sigma_{MN}} \int_{-\infty}^{\infty} (u_{st}\, v_{st}\, \eta_{st})^*\, \mathcal{N}_k \begin{pmatrix} u_{MN} \\ v_{MN} \\ \eta_{MN} \end{pmatrix} dy, \qquad st \neq MN. \tag{21}$$

At $O(\epsilon^2)$,

$$\sigma_2 = -i \sum_{s,t} A^1_{st} \int_{-\infty}^{\infty} (u_{MN}\, v_{MN}\, \eta_{MN})^*\, \mathcal{N}_k \begin{pmatrix} u_{st} \\ v_{st} \\ \eta_{st} \end{pmatrix} dy, \tag{22}$$

$$A^2_{st} = \frac{1}{\sigma_{st} - \sigma_{MN}} \left[\sigma_1 A^1_{st} + i \sum_{p,q} A^1_{pq} \int_{-\infty}^{\infty} (u_{st}\, v_{st}\, \eta_{st})^*\, \mathcal{N}_k \begin{pmatrix} u_{pq} \\ v_{pq} \\ \eta_{pq} \end{pmatrix} dy \right], \quad st \neq MN. \tag{23}$$

The above expressions are general for all equatorial waves. In principle, all wave types can contribute to the modification of a particular eigenmode, indeed all are required for

completeness of the basis. Nevertheless, the inverse frequency difference that leads the expressions for the expansion coefficients appears to limit the contributions to modes of a similar wave type (a point also made by Proehl, 1990). In our long-Rossby-wave calculations, we find that the contributions to (19) of the inertia-gravity modes ($n=1$, 3) are negligible.

a. Symmetry considerations

If $\widehat{U}$ (and consequently $\widehat{\delta H}$) is symmetric about the equator, then multiplying a Hermite basis vector of a particular y-symmetry by $\mathcal{N}_k$ will produce a new vector with the same symmetry. This is most easily seen by considering the symmetric part of the background field, $\widehat{U}_S = [\widehat{U}(y)+\widehat{U}(-y)]/2$ and $\widehat{\delta H}_S = [\widehat{\delta H}(y)+\widehat{\delta H}(-y)]/2$, with the corresponding operator $\mathcal{N}_{kS} = \mathcal{N}_k(\widehat{U}_S,\, \widehat{\delta H}_S)$, and defining the product

$$\begin{pmatrix} a \\ b \\ c \end{pmatrix} = \mathcal{N}_{kS} \begin{pmatrix} u_+ \\ v_- \\ \eta_+ \end{pmatrix} = ik\widehat{U}_S \begin{pmatrix} u_+ \\ v_- \\ \eta_+ \end{pmatrix} + \begin{pmatrix} (\widehat{U}_S)'\, v_- \\ 0 \\ ik\widehat{\delta H}_S\, u_+ + (\widehat{\delta H}_S\, v_-)' \end{pmatrix}. \tag{24}$$

In (24), $(u_+,\, v_-,\, \eta_+)^T$ represents a basis vector of a particular symmetry, where the $_+$ subscript can represent either a y-symmetric or a y-antisymmetric field, while the $_-$ subscript represents the opposite symmetry. Multiplication of the basis vector by $\widehat{U}_S$ (first term on the rhs) clearly leaves the symmetry of the vector unchanged. In the second term on the rhs, $(\widehat{U}_S)'$ is antisymmetric, so $(\widehat{U}_S)'\, v_-$ has the same symmetry as u_+. Likewise, both $\widehat{\delta H}_S\, u_+$ and $(\widehat{\delta H}_S\, v_-)'$ have the same symmetry as η_+, so the product vector $(a\, b\, c)^T$ has the same symmetry as the basis vector $(u_+\, v_-\, \eta_+)^T$.

A similar analysis shows that if $\widehat{U}$ is antisymmetric in y ($\widehat{U} = \widehat{U}_A$ and $\mathcal{N}_k = \mathcal{N}_{kA}$), then multiplication of an eigenvector by $\mathcal{N}_k$ changes the symmetry. Consequently, the operator $\mathcal{N}_k$ can be thought of as having the same y-symmetry as $\widehat{U}$ (note that we refer to the operational effect of $\mathcal{N}_k$ on the basis vectors and not to the matrix symmetry of $\mathcal{N}_k$).

If $\mathcal{N}_k$ ($\widehat{U}$) is symmetric and $(u_{st}\, v_{st}\, \eta_{st})$ has the opposite symmetry to our $O(1)$ solution,

$(u_{MN}\ v_{MN}\ \eta_{MN})$, then the integrand in (21) will be antisymmetric and A^1_{st} will vanish. At $O(\epsilon)$, therefore, the symmetric part of $\widehat{U}$ produces only eigenfunction corrections that have the same symmetry as the $O(1)$ solution, a point that was made by Ripa and Marinone, 1983. Conversely, the antisymmetric part of $\widehat{U}$ will result in $O(\epsilon)$ contributions that have the opposite symmetry to the $O(1)$ solution. Asymmetries in the eigenfunctions can thus be produced at $O(\epsilon)$ only by the anti-symmetric part of $\widehat{U}$. By the same logic we see in (20) that only the symmetric part of $\widehat{U}$ can contribute to changes in the dispersion relation at $O(\epsilon)$.

At $O(\epsilon^2)$, both the symmetric and antisymmetric parts of $\widehat{U}$ can contribute to the frequency correction. Suppose that $\mathcal{N}_k$ has an antisymmetric part which generates an $O(\epsilon)$ eigenfunction correction $A^1_{st}(u_{st}\ v_{st}\ \eta_{st})$ that has the opposite symmetry to the the $O(1)$ solution $(u_{MN}\ v_{MN}\ \eta_{MN})$. In (22), the antisymmetric part of $\mathcal{N}_k$ operating on $(u_{st}\ v_{st}\ \eta_{st})$ will produce a vector with the same symmetry as $(u_{MN}\ v_{MN}\ \eta_{MN})$, resulting in a symmetric integrand. There will be a non-zero contribution to the frequency modification at $O(\epsilon^2)$ due to the interaction of the antisymmetric part of the mean current with the asymmetrizing mode st.

We can think of the situation heuristically as an interaction in which a local contribution to the phase-speed change depends on both the local strength of the mean-current's phase-speed changing mechanism and the local relative magnitude of the wave vector. At $O(1)$, the magnitudes of all the Hermite eigenvectors are symmetric about the equator, and phase-speed altering aspects of the mean flow that are antisymmetric about the equator cancel themselves in the integral, producing no net effect. Once an asymmetry is introduced in the wave vector, however, the effect of the antisymmetric part of $\widehat{U}$ will no longer balance between the two hemispheres, and a net change in phase speed will result. The asymmetry introduced in the wave vector at $O(\epsilon)$ allows both the antisymmetric and the symmetric part of $\widehat{U}$ to affect the phase speed at $O(\epsilon^2)$.

More generally, the $O(\epsilon)$ solution gives us only the effect on phase speed of the interaction

between the background currents and the *unmodified* wave vectors. As the wave vectors themselves are changed, we must consider the interaction between the background currents and the *distorted* wave vectors, whether or not the distortions involve asymmetries. This effect enters into the perturbation solution only at $O(\epsilon^2)$.

4. Perturbation Solutions

In the following discussions, the $O(\epsilon^p)$ *correction* to frequency, for instance, refers to either σ_p or $\sigma_p \epsilon^p$, with the context making the choice clear. The $O(\epsilon^p)$ frequency *solution*, on the other hand, refers to $\sigma = \sum_{q=0}^{p} \sigma_q \, \epsilon^q$. The $O(1)$, $O(\epsilon)$ and $O(\epsilon^2)$ perturbation solutions with $\epsilon \widehat{U} = U(140W, y)$ and $\epsilon \widehat{U} = U(170W, y)$ are displayed in figs. 5 through 7. The numerical solutions from section 2 are also displayed as "ground truths." In fig. 5 we see that the small change in mode-2 phase speed at $170W$ is reproduced quite well by the $O(\epsilon)$ solution. In the other scenarios there is a larger change in phase speed and the $O(\epsilon)$ solution overestimates the change. At $O(\epsilon^2)$, the match is quite good between the perturbation and numerical solutions in all cases.

Figure 6 shows the $140W$ η, u and v eigenfunctions, with (19) summed up to $m = 20$ for both the $O(\epsilon)$ and the $O(\epsilon^2)$ corrections. The $O(\epsilon)$ solution anticipates the sense in which the eigenfunctions are distorted, but underestimates the magnitude in each case. The $O(\epsilon^2)$ solution provides a reasonable match with the numerical solutions, although it does not quite capture the extent of the asymmetry in the mode-1 η eigenfunction and some of the smaller-scale distorions of the u eigenfunction. Most of the η and v distortion is captured by summing (19) up to only $m = 5$ (not shown), with higher-mode contributions necessary only for a reasonable match of the u eigenfunction.

The eigenfunction solutions for $U(170W, y)$ are displayed in fig. 7, with thirty Rossby modes contributing to the perturbation solutions. The small asymmetry and poleward shift of the η peaks are produced by a few low-mode contributions, but the broadening of the

northern η peaks and the small-scale structure in u require the contributions of modes between 10 and 30. Summing (19) up to $m = 300$ does not visibly improve the eigenfunction approximations at either $140W$ or $170W$.

At $170W$ the $O(\epsilon^2)$ corrections are appropriately an order of magnitude smaller than the $O(\epsilon)$ corrections, but at $140W$ the two corrections are the same order of magnitude. A series of comparisons between numerical and perturbation solutions for weaker mean currents at $140W$ (not shown) demonstrated that the $O(\epsilon)$ solution matches the numerical solution well for $\epsilon\widehat{U} \leq 0.2\,U(140W, y)$ and that the $O(\epsilon^2)$ solution follows the numerical solution smoothly for progressively stronger currents up to $\epsilon\widehat{U} = U(140W, y)$. The $O(\epsilon^2)$ solution is thus providing an accurate estimate in the presence of the current systems we are considering, but we note that the $O(\epsilon^2)$ correction is providing more than just a small adjustment of the approximation. In the frequency solutions at $140W$, for instance, we argue that the change in tendency of the correction from $O(\epsilon)$ to $O(\epsilon^2)$ is evidence that the $O(\epsilon^2)$ correction provides a fundamental addition to the dynamics, presumably by introducing the influence of the wave-structure asymmetrization.

5. Physical mechanisms for phase speed modification

With some confidence that the perturbation solution reproduces the important modifications of long Rossby waves by mean currents typical of the equatorial Pacific, we turn now to extracting physical insight from the equations for the frequency correction.

a. $O(\epsilon)$ correction

Carrying out the multiplications in (20), we have

$$\frac{\sigma_1}{k} = \int_{-\infty}^{\infty} \widehat{U}\left(|u_0|^2 + |v_0|^2 + |\eta_0|^2\right) dy - \frac{i}{k}\int_{-\infty}^{\infty}\left(\widehat{U}' u_0^* + \widehat{\delta H}'\,\eta_0^*\right) v_0\, dy - \frac{i}{k}\int_{-\infty}^{\infty} \widehat{\delta H}\,\eta_0^*\,\nabla\cdot\underline{u}_0 dy. \quad (25)$$

This relation was derived by Ripa and Marinone, 1983, and a similar one by Proehl, 1990, in his model with both meridional and vertical structure. The first integral on the rhs is clearly the effect of advection by the mean current. Were the current uniform in y, this term would just be the Doppler shift $k\widehat{U}$ (remembering that $\int(|u_0|^2 + |v_0|^2 + |\eta_0|^2)\,dy = 1$). The form of this term points to an important principle: it is not just the strength of the mean current that matters, but how it projects onto the total wave field, $(|u_0|^2 + |v_0|^2 + |\eta_0|^2)$. In the case of short Rossby waves (as demonstrated by Ripa and Marinone, 1983) the net advection is determined by the projection of the mean current onto the squared meridional velocity structure, since this component dominates the wave vector. For long Rossby waves, however, $|v_0| \ll |u_0|$ and the net advection is determined by the projection of $\widehat{U}$ onto $(|u_0|^2 + |\eta_0|^2)$. Proehl, 1990, appears to have concluded similarly, but his results are easy to misinterpret as emphasizing the projection of $\widehat{U}$ onto $|v_0|^2$ (McPhaden and Ripa, 1990). The difference is significant because the symmetry of v_0 is opposite to that of both u_0 and η_0. For even meridional mode numbers, $|v_0|^2$ will have an extremum at the equator coinciding with the strong but narrow EUC, while $|u_0|^2 + |\eta_0|^2$ will be negligible there. For odd mode numbers the opposite is true. Consequently, the EUC will advect odd modes quite differently than even modes, and a long Rossby wave of a given mode number quite differently than the short Rossby wave of the same mode number.

The meaning of the second integral in (25) is less clear, and our interpretation of it is a major difference between this and previous work. This is the term consistent with the mechanism cited by Proehl, 1990, involving the advection of background momentum and density fields by the meridional circulation of the wave field. Although Proehl's description fits the form of the integrand, it is not obvious how this mechanism contributes to the wave frequency. We prefer to reorganize this term to reflect mean-current modification of the background pv field, which has been demonstrated in mid-latitude dynamics to influence the Rossby wave speed.

Using the relationships between the wave-vector components implicit in the shallow-water

equations, the geostrophy of the mean current and the vanishing of $\widehat{U}$ and the wave fields as $|y| \to \infty$, (25) can be rewritten

$$\frac{\sigma_1}{k} = \int_{-\infty}^{\infty} \widehat{U}\left(|u_0|^2 + |v_0|^2 + |\eta_0|^2\right)\, dy + \int_{-\infty}^{\infty} \widehat{\delta H}\left(\eta_0^* u_0 + \frac{\sigma_0}{k}|v_0|^2\right)\, dy$$

$$- \int_{-\infty}^{\infty} \widehat{\delta Q}' \frac{|v_0|^2}{2(k^2 - \sigma_0^2)}\, dy \quad - \quad \frac{\sigma_0}{k}\int_{-\infty}^{\infty} \widehat{\delta(Q^2)} \frac{|v_0|^2}{2(k^2 - \sigma_0^2)}\, dy. \tag{26}$$

In (26), $\widehat{\delta Q}'$ and $\widehat{\delta(Q^2)}$ are the $O(\epsilon)$ corrections to the pv gradient and the squared pv field,

$$\widehat{\delta Q}' = -\widehat{U}'' - \left(y\,\widehat{\delta H}\right)', \tag{27}$$

$$\widehat{\delta(Q^2)} = -2y(\widehat{U}' + y\,\widehat{\delta H}), \tag{28}$$

where we have expanded the pv and squared pv fields in powers of ϵ:

$$Q = \frac{y - \epsilon\widehat{U}'}{1 + \epsilon\,\widehat{\delta H}} = Q_0 + \epsilon\,\widehat{\delta Q} + O(\epsilon^2), \tag{29}$$

$$Q^2 = Q_0^2 + \epsilon\,\widehat{\delta(Q^2)} + O(\epsilon^2), \tag{30}$$

and $Q_0 = y$. The pv normalization is $Q_* = (\sqrt{\beta c}/H_0)Q$, where the $_*$ subscript denotes a dimensional variable.

No approximations have been made in going from (25) to (26), but the reorganization is not unique and requires some justification. The origin of the advection (Doppler shift) term is clear and that has been left unchanged. We expect Rossby-wave phase speed to be related to the strength of the pv gradient, but the gradient matters only to the extent that it parallels the wave velocities. The natural projection for $\widehat{\delta Q}'$, therefore, is onto $|v_0|^2$, and our reorganization was guided by this premise to produce the 3rd term on the rhs of (26). Extracting this term constrains the forms of the other terms, but some elementary considerations lend credence to their reasonableness.

By using the mid-latitude definition of the y_*-dependent, inverse-square deformation radius,

$$L_{d^*}^{-2} = (\beta y_*/c)^2, \tag{31}$$

and defining a y_*-dependent, dimensional meridional wavenumber, $l_*(y_*)$, that obeys

$$l_*^2\, v_* = -d^2 v_*/dy_*^2, \tag{32}$$

we can write the dimensional dispersion relation for classical (rest-state) equatorial Rossby waves ($\sigma_*^2/c^2k_*^2 \ll 1$) in a way that resembles the mid-latitude dispersion relation. The dimensional (starred subscripts) and corresponding nondimensional dispersion relations are

$$\sigma_* = \frac{-\beta\, k_*}{k_*^2 + l_*^2(y_*) + L_{d^*}^{-2}(y_*)}, \tag{33}$$

$$\sigma = \frac{-Q_0'\, k}{k^2 + l^2(y) + Q_0^2(y)}. \tag{34}$$

The nondimensional Q' and Q^2 fields clearly represent β and $L_{d^*}^{-2}$ in the rest-state dynamics. The latter term is not typically found in the dispersion relations of equatorial modes, but Ripa, 1994, showed that the classical equatorial-mode solutions could be reproduced by a ray-tracing solution using the dispersion relation (33). The classical equatorial-mode dispersion relation is thus influenced by the integrated effect of $L_{d^*}^{-2}$, and it is reasonable to expect mean-current modifications of the dispersion relation to be influenced by the integrated effect of the mean-current modifications of $L_{d^*}^{-2}$, which we in turn expect to be related to $\widehat{\delta(Q^2)}$.

The second integral on the rhs of (26), with $\widehat{\delta H}$ in the integrand, apparently represents the projection of the y-dependent, local gravity-wave speed onto the dominant features of the wave structure, an interpretation which is supported by a simple thought experiment. Imagine a case where $\widehat{U} = 0$ and $\widehat{\delta H}$ is a constant. This would represent a no-mean-flow case for which we have an analytical solution, but where we have nondimensionalized by the wrong layer thickness and hence the wrong value of c. In the high frequency gravity-wave limit, the two pv-related integrals are negligible and the second integral in (26) reduces to $\widehat{\delta H}/2$, which is the proper $O(\epsilon)$ correction to c: $[g'H_0]^{1/2} \rightarrow [g'H_0(1 + \epsilon\, \widehat{\delta H})]^{1/2}$.

The $\widehat{\delta H}$ integral remains large in the long-Rossby-wave limit, but we expect changes in the gravity-wave speed to affect the Rossby-wave speed only through the manner in which these changes affect the pv field. For the most efficient analysis of Rossby waves, therefore,

we expect this integral to be absorbed into one or both of the pv-related integrals. In our nondimensional scheme, the forms for the "effective β" and "effective deformation radius" in the mean-current analysis of Chang and Philander, 1989, are $\beta_{eff} = (Q_0/Q)Q'$ and $L_{d\ eff}^{-2} = (Q_0/Q)Q^2$. The formulation used to derive these terms is not strictly applicable to equatorial modes, but the forms of the terms suggest that the dynamically important aspects of the mean current field may be related to but not precisely equal to Q' and Q^2. Forcing our perturbation solution to produce the β_{eff} and $L_{d\ eff}^{-2}$ forms of Chang and Philander, 1989, produces extraneous terms that have no clear physical meaning, and we elect rather to reorganize the $\widehat{\delta H}$ integral to merge with the pv-related terms in the manner that best preserves the physics-related forms of these latter terms.

At this point we introduce approximations to (26) that are appropriate for long Rossby waves, where $\sigma_0 \ll 1$, $k \ll 1$, $(\sigma_0/k)^2 \ll 1$, $\langle|v_0|^2\rangle \ll \langle|u_0|^2\rangle$, and

$$\frac{1}{2(k^2-\sigma_0^2)} \sim -\frac{\langle|u_0|^2\rangle}{\langle|v_0|^2\rangle}\,\frac{\sigma_0}{k}. \tag{35}$$

The angle brackets indicate integration over the domain. In the long-Rossby-wave limit, $\langle\widehat{\delta H}\,\eta_0^* u_0\rangle$ can be approximated as

$$\langle\widehat{\delta H}\,\eta_0^* u_0\rangle \sim \frac{\langle|u_0|^2\rangle}{\langle|v_0|^2\rangle}\left[\frac{\sigma_0}{k}\Big(2\langle\widehat{\delta H}\,|v_0|^2\rangle - \langle(y\widehat{\delta H})'|v_0|^2\rangle\Big) + \Big(\frac{\sigma_0}{k}\Big)^2\Big(\langle y\widehat{U}'|v_0|^2\rangle + \langle\widehat{U}|v_0|^2\rangle\Big)\right]. \tag{36}$$

Up to now we have applied approximations only to coefficients, and as a final step we will neglect two terms that are small in the long-Rossby-wave limit: the final term in (36), which is $O([\sigma_0/k]^2)$ relative to the important Doppler shift terms, and the last term in the first line of (26), $(\sigma_0/k)\langle\widehat{\delta H}\,|v_0|^2\rangle$, which is $O(\langle|v_0|^2\rangle/\langle|u_0|^2\rangle)$ relative to $\langle\widehat{\delta H}\,\eta_0^* u_0\rangle$. Equation (26) can now be rewritten in what we propose to be the most illuminating form for analysis of the $O(\epsilon)$, long-Rossby-wave phase-speed modification by the mean currents:

$$\frac{\sigma_1}{k} = \Big\langle\widehat{U}\big(|u_0|^2+|v_0|^2+|\eta_0|^2\big)\Big\rangle + \langle|u_0|^2\rangle\left[\frac{\sigma_0}{k}\frac{\Big\langle\widehat{\delta\beta}_{eff}|v_0|^2\Big\rangle}{\langle|v_0|^2\rangle} + \Big(\frac{\sigma_0}{k}\Big)^2\frac{\Big\langle\widehat{\delta L_d^{-2}}_{eff}\,|v_0|^2\Big\rangle}{\langle|v_0|^2\rangle}\right], \tag{37}$$

where

$$\widehat{\delta\beta}_{eff} = \widehat{\delta Q}' + \widehat{\delta H} - y\widehat{\delta H}' = -(\widehat{U}'' + 2y\widehat{\delta H}'), \quad (38)$$

$$\widehat{\delta L_d^{-2}}_{eff} = \widehat{\delta(Q^2)} + y\widehat{U}' = -y(\widehat{U}' + 2y\widehat{\delta H}). \quad (39)$$

An inspection of fig. 1 shows that δH is slightly smaller than U, and that the meridional scale of the EUC is between 1/2 and 1 equatorial deformation radius while the scales of the other currents are typically around 1 deformation radius. We can thus expect that $|U| \leq |U'| \leq |U''|$, but we would not expect the various mean-current related terms in (37) to differ by more than perhaps one order of magnitude. Although $\langle|v_0|^2\rangle \ll \langle|u_0|^2\rangle$ in the long-wave limit, the coefficient $\langle|u_0|^2\rangle/\langle|v_0|^2\rangle$ in front of the pv-related integrals in (37) makes them potentially of the same order as the advective integral. Indeed, this coefficient keeps the ratio of the pv-to-advective integrals relatively constant throughout the long-wave frequency range, even as the ratio $(\langle|u_0|^2\rangle/\langle|v_0|^2\rangle)$ changes by many orders of magnitude. For meridional mode m, $\sigma_0/k = -1/(2m+1)$, so for low modes all of the terms in (37) can potentially play a role in the phase-speed modification, depending on the relative magnitudes of the mean-current features and how they project onto the wave functions. Because of the smaller meridional scale of the EUC, we expect the U'' contribution to $\widehat{\delta\beta}_{eff}$ to be particularly important near the equator.

b. $O(\epsilon)$ solutions at $140W$ and $170W$

The $O(\epsilon)$ relative frequency corrections for meridional-mode-1 and -2 long Rossby waves in the presence of $140W$ and $170W$ mean currents are listed in the second column of Table 1. Columns three through six list the contributions of the separate terms in (37), with each column header identifying the mean-current feature(s) in the integrand of the relevant term. The $\widehat{\delta\beta}_{eff}$ term has been separated into two components: the effect of the mean-current curvature, $\widehat{U}''$, and the effect of the interface slope, $y\,\widehat{\delta H}'$.

All of the terms make noticeable contributions, but in general the frequency change is

dominated by advection ($\widehat{U}$) and the pv-gradient modification due to $\widehat{U}''$, with the latter term accounting for over 40% of the frequency shift in each case. Interestingly, these terms both contribute to the decrease in the mode-1 phase speed and also to the increase in the mode-2 phase speed at $140W$. At $170W$, both terms also contribute to the marked decrease in mode 1 phase speed, but they are both rather small and act counter to each other for mode 2.

Table 1 was compiled for the annual period, but over the range (60 days $< T <$ 3 years) the values represented in Table 1 change by at most a few percent. What small changes occur do so at the higher frequencies and are likely due to the $|v_0|^2$ term beginning to influence the advective integral.

c. Graphical analysis of the $O(\epsilon)$ correction

Figs. 8 through 11 present a graphical breakdown of the two dominant terms in Table 1, advection (left column) and $\widehat{U}''$-pv-gradient modification (right column), with each figure representing one of the meridional modes at one longitude. The three panels in each column are arranged to illustrate the projection of the mean-current feature onto the important part of the mode-dependent wave structure. The top panel shows the meridional structure of the relevant mean-current feature ($U = \epsilon\widehat{U}$ or U''), emphasizing the symmetric part (the dynamically important part at $O(\epsilon)$). The middle panel shows the structure of the relevant $O(1)$ wave component; $(|u_0|^2 + |v_0|^2 + |\eta_0|^2)$ in the case of advection and $|v_0|^2$ in the case of pv-gradient modification. The bottom panel shows the appropriately scaled product of the above two terms, which is the integrand of the relevant term in (37). A positive integral of the curve in the bottom left panel indicates net advection in the positive-x direction, or a slowing of the long-Rossby wave's westward phase speed. A positive U'' decreases the strength of the pv gradient and also slows the Rossby wave, so a net positive (negative) area under the curve in the bottom right panel acts on the phase speed with the same tendency

as a net positive (negative) area under the curve in the bottom left panel. The bottom panels of both columns in all figures are scaled identically to facilitate comparison of the latitude-dependent dynamical effects between modes and between current systems.

We are now ready to extract some physical insight from the form of the $O(\epsilon)$ frequency correction. The narrow, equatorially centered, eastward EUC dominates the equatorial current system at 140W (fig. 8, top left panel), but the symmetric part of the westward SEC has a maximum amplitude that is roughly 40% that of the EUC (with peaks near $3S$ and $3N$), and a total meridional span that is more than twice that of the EUC. Consequently, the net advection could easily be eastward, westward or negligible, depending on how the meridional distribution of the combined wave-component amplitudes (fig. 8, middle left panel) lines up with the currents. The combined amplitudes of mode 1 have a broad meridional span because of the off-equatorial peaks in η_{12} but also a pronounced equatorial peak because of the equatorial maximum of u_{12}. As a result of this peak, the eastward advection by the EUC overpowers the westward advection by the SEC, and the mode-1 westward phase speed is decreased by the advective mechanism. The eastward NECC plays a minor role in changes at the $O(\epsilon)$ level because of its strong asymmetry, and particularly at $140W$ because of its high latitude.

The rapid change in shear at the core of the EUC dominates the U'' profile, with a negative extremum on the equator (fig. 8, upper right panel), but the positive curvature associated with the peaks in the SEC (or alternately the flanks of the EUC) remains significant, with peaks near $2S$ and $2N$. In fact, because the meridional velocity of mode 1 has a zero on the equator (middle right panel), the marked increase in the background pv gradient at the center of the EUC has almost no effect on this mode. Although the increase in the gradient is large, it is confined to a narrow latitudinal strip where wave motions do not parallel the gradient. By contrast, the amplitude of the wave's meridional velocity is close to its maximum at the latitudes where the background pv gradient is decreased near the peaks in the SEC. Consequently, the dominant pv-gradient modification by the mean current system

acts to slow down mode 1, in concert with the advection by the mean current.

In the case of mode 2 (fig. 9), η and u have zeros on the equator, so the strong EUC has very little advective effect on the mode. The off-equatorial maxima in η and u coincide quite well with the maxima in the westward SEC, so the advective mechanism acts to increase the westward phase speed of mode 2. The off-equatorial maxima of mode 2's meridional velocity (middle right panel) are somewhat poleward of, and do not overlap well with, the maxima in U'' near the peaks of the SEC. On the other hand, $|v_{22}|$ has a local maximum on the equator where the increase in the background pv gradient associated with the peak of the EUC is at its maximum. Consequently, the dominant pv-gradient-modifying mechanism of the mean currents also acts to increase the phase speed of mode 2.

At $170W$ (figs. 10 and 11) the EUC is somewhat weaker and wider than at $140W$. Its integrated advective effect is comparable at the two longitudes, but the associated pv-gradient increase on the equator is significantly weaker at $170W$. The lack of a northern branch to the SEC at $170W$, combined with a more equatorward core of the NECC, significantly decreases the net potential for westward advection compared to $140W$. The small-scale current structure between the EUC and the NECC introduces comparable structure to U_s'' at these latitudes, but the southern branch of the SEC still biases the fluctuations to a net positive U_s'' in the region. Nevertheless, the more equatorward location of the NECC's core brings a significant negative U_s'' peak closer to the region where it overlaps with the meridional velocity structure of modes 1 and 2.

The net eastward advective effect of the EUC on mode 1 at $170W$ appears to be roughly equivalent to that at $140W$ because the smaller amplitude at $170W$ is offset by the increased width. The significantly weaker westward advective effect of the SEC at $170W$, however, results in a larger net eastward advection of mode 1 at $170W$ than at $140W$ (compare bottom panels, figs. 10 and 8). The localized increase in the pv gradient due to the current structure between the EUC and the NECC at $170W$ combines with the more equatorward position of the NECC's increased pv gradient contribution to partially counter the slowing effect of

the SEC's decrease in the pv gradient. Consequently, the net slowing effect on mode 1 of the U_s''-associated pv-gradient modification is somewhat smaller at $170W$ than at $140W$. The net effect of the changes in advective potential and pv-gradient modification is that the $O(\epsilon)$ phase speed of mode 1 at $170W$ is very similar to that at $140W$, although for slightly different physical reasons.

At $140W$ the narrow EUC had very little overlap with $(|\eta_{22}|^2 + |u_{22}|^2 + |v_{22}|^2)$ and the advection of mode 2 was almost all westward due to the SEC. At $170W$, the wider EUC results in a slightly larger contribution to eastward advection of mode 2 (compare bottom left panels, figs.11 and 9). As noted, the absence of the northern branch of the SEC at $170W$ decreases the potential for westward advection, and the net effect is a small eastward advection of mode 2 at $170W$. The net effect of the pv-gradient modification at $170W$ is still to speed up the westward phase speed of mode 2, but the effect is only about half as strong as at $140W$, due to the decreased strength and increased width of the EUC at $170W$. In the net, there is a relatively insignificant increase in the phase speed of mode 2 at $170W$.

d. $O(\epsilon^2)$ correction

The analysis of the previous section has given us some insight into how the mean currents act upon the Hermite wave vectors to modify the phase speed, and these insights are all we need for a relatively weak current system; for instance one that has the structure of the $140W$ currents but only 1/4 of the full strength. In this case, the changes to the eigenfunctions are minimal and the $O(\epsilon)$ correction captures the essence of the dispersion-relation modification (not shown).

When the currents are stronger, however, the wave vectors being acted on by the mean current are significantly different from the Hermite wave vectors, and this is when the $O(\epsilon^2)$ frequency correction becomes important. By changing the order of summation and integra-

tion, (22) can be rewritten

$$\sigma_2 = -i \int_{-\infty}^{\infty} (u_0\, v_0\, \eta_0)^*\, \mathcal{N}_k \begin{pmatrix} u_1 \\ v_1 \\ \eta_1 \end{pmatrix} dy. \tag{40}$$

The $O(\epsilon^2)$ solution can be written

$$\sigma = \sigma_0 + \epsilon \Delta\sigma, \tag{41}$$

where

$$\Delta\sigma \equiv \sigma_1 + \epsilon\sigma_2 = -i \int_{-\infty}^{\infty} (u_0\, v_0\, \eta_0)^*\, \mathcal{N}_k \begin{pmatrix} (u_0 + \epsilon u_1) \\ (v_0 + \epsilon v_1) \\ (\eta_0 + \epsilon \eta_1) \end{pmatrix} dy. \tag{42}$$

Equation (42) demonstrates a similarity between the full frequency correction in the $O(\epsilon^2)$ solution and the $O(\epsilon)$ correction that we have just analyzed (compare (42) with (20)), except that both the $O(1)$ and $O(\epsilon)$ wave-vector solutions are now important.

In general, the analyses of the individual mechanisms is more complex than our $O(\epsilon)$ analyses, but an approximation to the Doppler shift takes a gratifyingly simple form. The form of (42) suggests that we consider a wave vector that is an average of the $O(1)$ and $O(\epsilon)$ solutions,

$$(\overline{u}\ \overline{v}\ \overline{\eta}) = (u_0\, v_0\, \eta_0) + \frac{\epsilon}{2}(u_1\, v_1\, \eta_1), \tag{43}$$

then we can rewrite (42) as

$$\begin{aligned} \Delta\sigma \;\; = \;\; & -i \int_{-\infty}^{\infty} (\overline{u}\ \overline{v}\ \overline{\eta})^*\, \mathcal{N}_k \begin{pmatrix} \overline{u} \\ \overline{v} \\ \overline{\eta} \end{pmatrix} dy \\ & -\frac{\epsilon}{2}\, i \int_{-\infty}^{\infty} \left[(u_0\, v_0\, \eta_0)^*\, \mathcal{N}_k \begin{pmatrix} u_1 \\ v_1 \\ \eta_1 \end{pmatrix} - (u_1\, v_1\, \eta_1)^*\, \mathcal{N}_k \begin{pmatrix} u_0 \\ v_0 \\ \eta_0 \end{pmatrix} \right] dy + O(\epsilon^2). \end{aligned} \tag{44}$$

We now consider only the advective part of $\mathcal{N}_k$:

$$\mathcal{N}_{kA} = ik\widehat{U}\, I = \mathcal{N}_k - \begin{pmatrix} 0 & \widehat{U}' & 0 \\ 0 & 0 & 0 \\ ik\widehat{\delta H} & (\widehat{\delta H}' + \widehat{\delta H}\frac{d}{dy}) & 0 \end{pmatrix}, \tag{45}$$

where I is the identity matrix. When $\mathcal{N}_{kA}$ is substituted for $\mathcal{N}_k$ in (44), the second integral on the rhs vanishes and

$$\frac{\Delta\sigma_A}{k} = \int_{-\infty}^{\infty} \widehat{U}(|\overline{u}|^2 + |\overline{v}|^2 + |\overline{\eta}|^2)\, dy + O(\epsilon^2). \tag{46}$$

To within the accuracy of the solution, the analysis of the full frequency correction due to advection in the $O(\epsilon^2)$ solution is identical to the analysis we performed at the $O(\epsilon)$ level, except what matters is how the mean current projects onto the *average* of the rest-state wave vector and the deformed wave vector of the $O(\epsilon)$ solution.

The $O(\epsilon^2)$ frequency correction at $170W$ is small compared to σ_0 for both modes (fig. 5), so we illustrate the above at $140W$ only in fig. 12, with the mode-1 advection illustrated in the left column and the mode-2 in the right. The format is similar but not identical to that of figs. 8-9. Only U is displayed in the top panel because both the symmetric and antisymmetric parts are important in this case. The middle panel displays the important parts of the average wave vector (43), with a subscript indicating the meridional mode number M. The thick curve in the bottom panel is again the product of the thick curves in the upper and middle panels and represents the integrand of (46). Only the symmetric part of the integrand contributes to the frequency correction, and this is shown as a thin line for direct comparisons with the integrands shown in the bottom left panels of figs. 8 and 9.

Comparing the left columns of figs. 8 and 12, we see that the important effect on the mode-1 wave vector is the broadening and northward shift of the zonal velocity peak. Because the EUC at $140W$ is centered slightly south of the equator, this decreases the eastward advective effect of the EUC while simultaneously increasing the westward advective effect of the SECN. Consequently, the relative slowing of the mode due to advection is reduced from 7% to 2%.

The northward shift of the u and η amplitudes also enhances the advective influence of the NECC but not enough to compensate for the loss of advection by the EUC.

A comparison of the right column of fig. 12 with the left column of fig. 9 shows that the enhancement and slight equatorward shift of mode-2's southern zonal-velocity peak enhances the advective effect of the EUC on this mode. Any decrease in the westward advection of the SECN appears to be compensated for by an increase in advection by the SECS, with net advection by the SEC changing little. In total, the relative increase in mode-2's westward phase speed by advection is decreased from 11% to 7%.

6. Summary

With numerical solutions, we have shown that the effects of zonal equatorial currents on long Rossby waves can be somewhat counterintuitive. The effect of the equatorial Pacific's strongest currents (at $140W$) on baroclinic mode 1 is to slow down meridional mode 1 but speed up meridional mode 2. The SSH signal of meridional mode 1 is weakened in the southern hemisphere and enhanced in the northern hemisphere, but the exact opposite is true for meridional mode 2.

A perturbation expansion solution showed that in the two current systems that we considered ($140W$ and $170W$) the dominant physical mechanisms affecting the Rossby-wave phase speeds are advection by the mean currents and modification of the background pv gradient by the curvature in the mean currents, $\hat{U}''$. The extent of the advective effect is determined by how well the mean current projects onto the wave-vector's squared magnitude, $|u|^2 + |v|^2 + |\eta|^2$ (dominated by $|u|^2 + |\eta|^2$), and the pv-gradient effect depends on how well $\hat{U}''$ projects onto the wave's squared meridional velocity, $|v|^2$.

The opposite effects on the phase speeds of modes 1 and 2 are due largely to a coincidence between the meridional scales of the currents and waves, and two characteristics of equatorial waves: 1) the meridional phases of modes 1 and 2 differ by 90° at the equator and 2) within

a single mode the zeros of v are staggered relative to those of u and η. Because of mode 1's zonal-velocity maximum on the equator, eastward advection by the EUC dominates a weaker westward contribution by the SEC for net eastward advection of the mode. By contrast, mode 2's zonal velocity and pressure have zeros on the equator while the zonal velocity has local extrema near the peaks in the SECS and SECN, thus subjecting this mode to strong westward advection.

The meridional velocity of mode 1 has a zero on the equator so that it is relatively unaffected by the large increase in the background pv gradient at the core of the EUC. The local extrema of mode 1's meridional velocity overlap well with the region of decreased pv gradient at the peaks of the SECS and SECN, however, contributing to a decreased phase speed. The meridional velocity of mode 2, on the other hand, has a local extremum on the equator where the pv gradient is enhanced, and zeros near the peaks of the SECS and SECN where the pv gradient is weakened; the pv-gradient modification thus acts in concert with advection to speed up mode 2.

At $170W$ the general picture for mode 1 is similar to the $140W$ scenario (see sec. 5b for details). For mode 2, however, the weaker pv-gradient enhancement due to a more diffuse EUC combined with weaker advection by a weaker SEC lead to very little change in the dispersion relation.

The above observations depend on the coincidence of wave and current structures, and the results would be quite different for a higher baroclinic mode with a smaller deformation radius. In that case, for instance, the off-equatorial meridonal-velocity extrema of mode 1 could conceivably overlap with the region of enhanced pv gradient near the equator so that the advective and pv-gradient effects on mode 1 might act counter to each other. Each mode clearly must be considered separately.

The preceding descriptions are also limited to relatively weak currents (up to $\sim 25\%$ of $U(140W)$) acting on wave vectors that have not changed significantly from the classical Hermite-function wave vectors. At mean-current magnitudes typical of the east-central Pa-

cific, distortions of the wave vectors can be significant, and can influence the interaction with the mean currents. We have shown that the analysis of the advective effect of the stronger currents on phase speed is identical to that described above, except that we must consider the projection of the mean current onto an average of the undistorted and the $O(\epsilon)$ distorted wave vectors. The interactions of the distorted wave-vectors with the changes in the pv field are more complicated.

With the phase-speed modification by the stronger currents so dependent on the nature of the wave-vector distortions, a better understanding of the controlling mechanics behind these distortions clearly is needed at this point. Boyd, 1978, found that an eastward equatorial jet produced an expansion of the meridional span of the wave vectors while a westward jet produced a contraction, and he attributed these effects to changes in the deformation radius due to U'. To our knowledge, no one has provided a satisfactory explanation for the striking wave-vector asymmetries that appear to be typical of the east-central Pacific. It is interesting to note that in the cases we have studied, the wave-vector distortions appear to lessen the impact on the dispersion relations. The $O(\epsilon^2)$ solutions represent an increase in the wave-vector distortions over the $O(\epsilon)$ solutions but a decrease in the phase-speed shift. Thus, important questions remain that warrant continued in-depth investigations.

Acknowledgments.

We thank Jay McCreary for suggesting the perturbation approach, Dennis Moore for guidance and inspiration, and Tom Farrar for many helpful discussions. The work was supported by NASA grant NNG05GN98G.

References

Boyd, J., 1978: The effects of latitudinal shear on equatorial waves, part II: applications to the atmosphere. *J. Atmos. Sci.*,**35**, 2259-2267.

Chang, P. and S.G.H. Philander, 1989: Rossby wave packets in baroclinic mean currents. *Deep-Sea Res.*, **36**, 17–37.

Chelton, D.B., R.A. deSzoeke, M.G. Schlax, K. El Naggar and N. Siwertz, 1998: Geographical variability of the first baroclinic Rossby radius of deformation. *J. Phys. Oceanogr.*, **28**, 433–460.

Chelton, D.B., M.G. Schlax, J.M. Lyman and G.C. Johnson, 2003: Equatorially trapped Rossby waves in the presence of meridionally sheared baroclinic flow in the Pacific Ocean. *Progress in Oceanography*, **56**, 323–380.

Johnson, G.C., B.M. Sloyan, W.S. Kessler and K.E. McTaggart, 2002: Direct measurements of upper ocean currents and water properties across the tropical Pacific during the 1990s. *Progress in Oceanography*, **52**,31–61.

Matsuno, T., 1966: Quasi-geostrophic motions in the equatorial area. *J. Met. Soc. Japan*, **44**, 25–42.

McPhaden, M.J. and R.A. Knox, 1979: Equatorial Kelvin and inertio-gravity waves in a zonal shear flow. *J. Phys. Oceanogr.*, **9**, 263–277.

McPhaden, M.J. and P. Ripa, 1990: Wave-Mean Flow Interactions in the Equatorial Ocean. *Ann. Rev. Fluid Mech.*, **22**,167–205.

Moore, D.W. and S.G.H. Philander, 1977: Modeling of the tropical ocean circulation. *The Sea*, **6**, 319–361. New York, John Wiley & Sons

Proehl, J.A., 1990: Equatorial wave-mean flow interaction: the long Rossby waves. *J. Phys. Oceanogr.*, **20**, 274–294.

Philander, S.G.H., 1979: Equatorial waves in the presence of the equatorial undercurrent. *J. Phys. Oceanogr.*, **9**, 254–262.

Ripa, P., 1994: Horizontal wave propagation in the equatorial waveguide. *J. Fluid Mech.*, **271**, 267–284.

Ripa, P. and S.G. Marinone, 1983: The effect of zonal currents on equatorial waves. *Hydrodynamics of the Equatorial Ocean*, C.J.C. Nihoul, Ed., Elsevier, 291–317.

Zheng, Q., X.-H. Yan and C.-R. Ho, 1994: The effects of shear flow on propagation of Rossby waves in the equatorial oceans. *J. Phys. Oceanogr.*,**24**, 1680–1686.

List of Figures

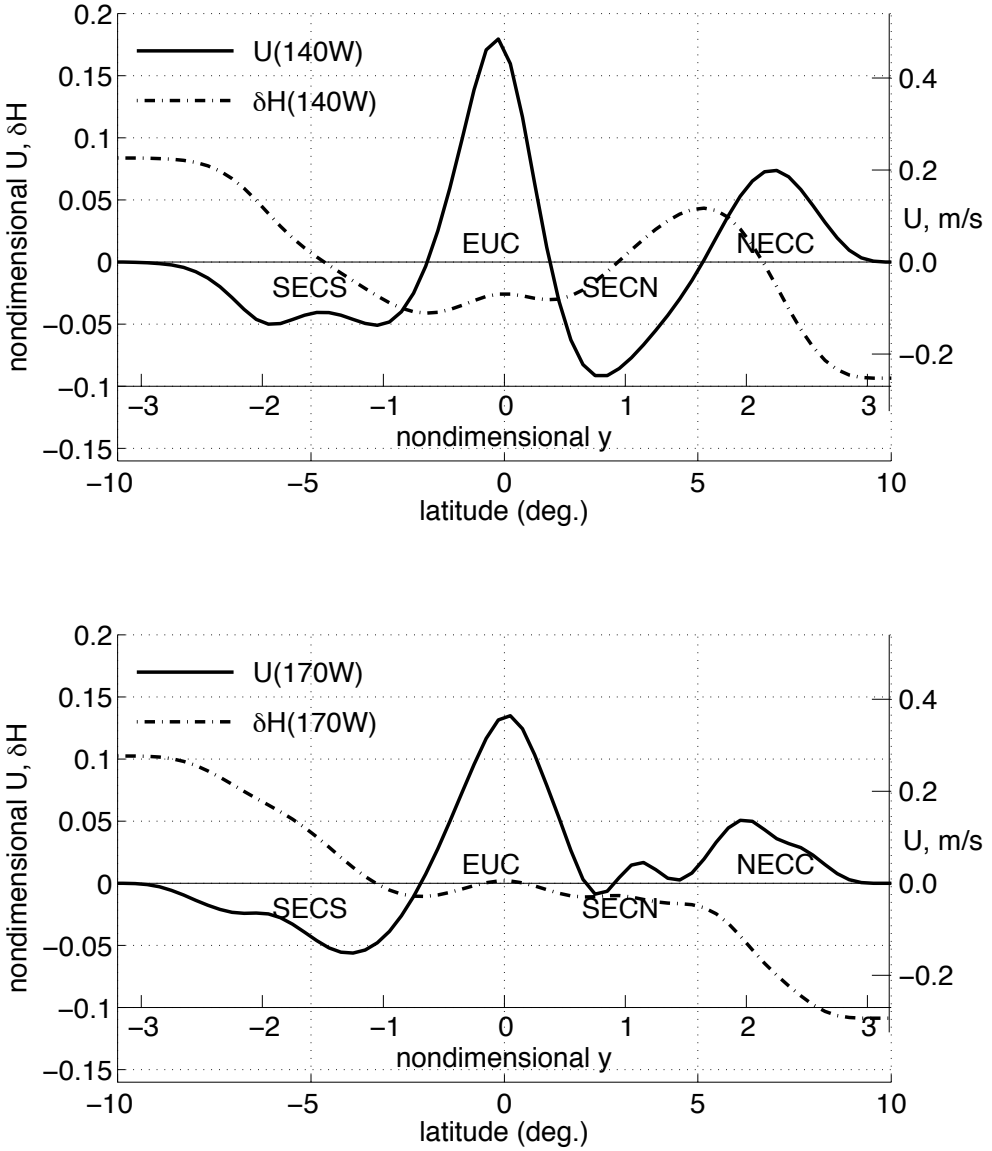

FIG. 1. Equatorial zonal-current systems at $140W$ (top panel) and $170W$ (bottom panel) from C03 (based on average zonal ADCP transects of Johnson et al., 2002.)

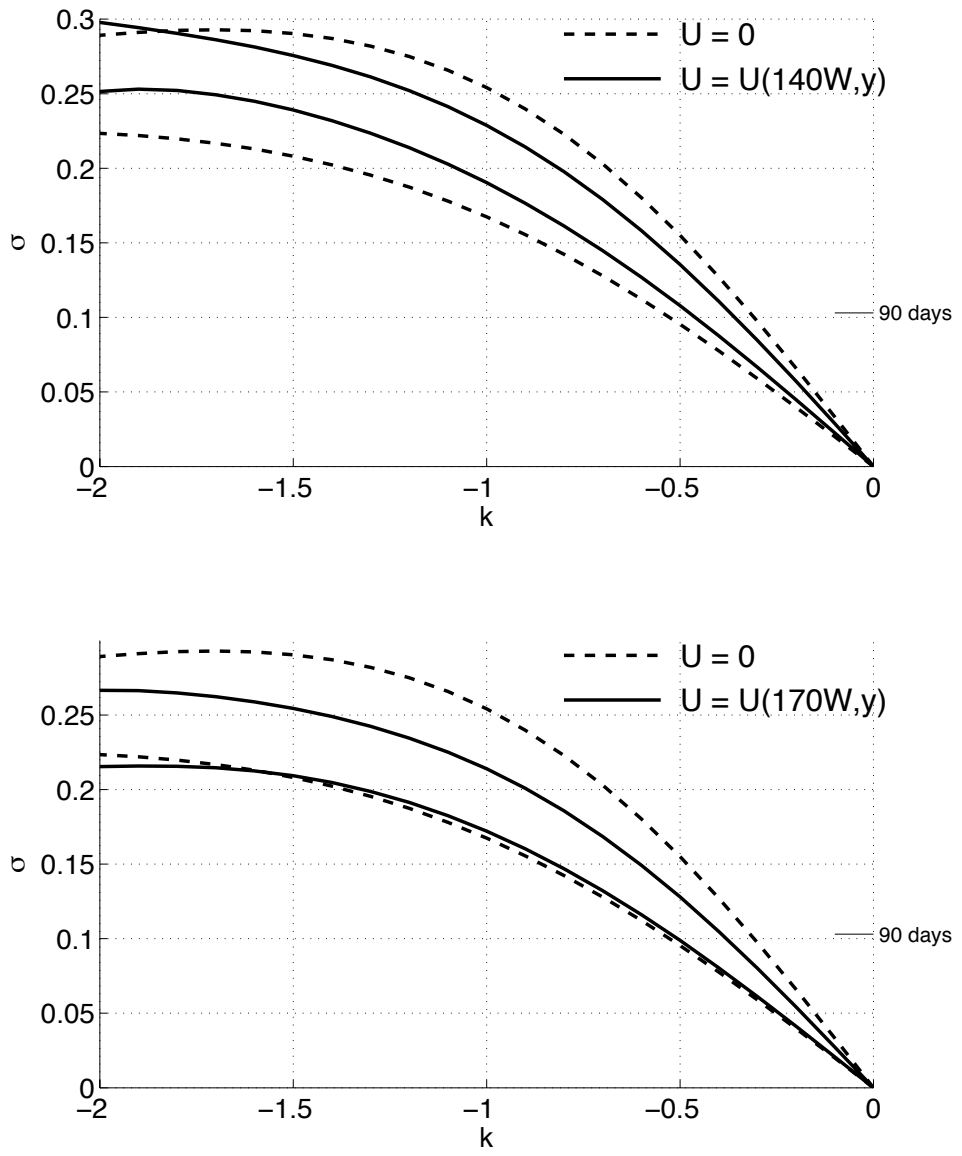

FIG. 2. Rossby-wave dispersion relations for the lowest two meridional modes at $140W$ (top panel) and $170W$ (bottom panel). Solid curves represent numerical solutions of shallow-water equations linearized about the mean currents. Dashed curves are classical solutions for no mean flow.

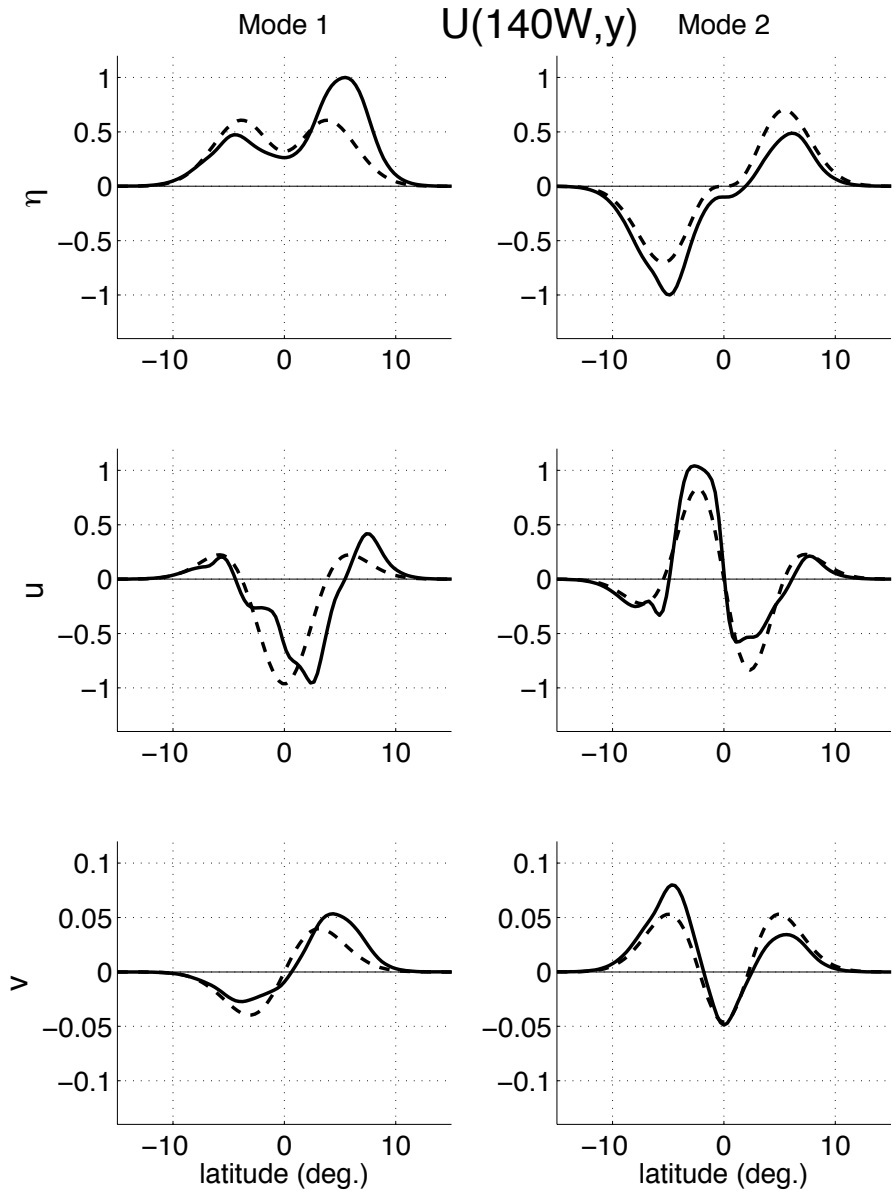

FIG. 3. Long-Rossby wave eigenfunctions at the annual period: meridional modes 1 (left column) and 2 (right column). Solid curves represent numerical solutions of shallow-water equations linearized about the currents at $140W$. Dashed curves are classical solutions for no mean flow.

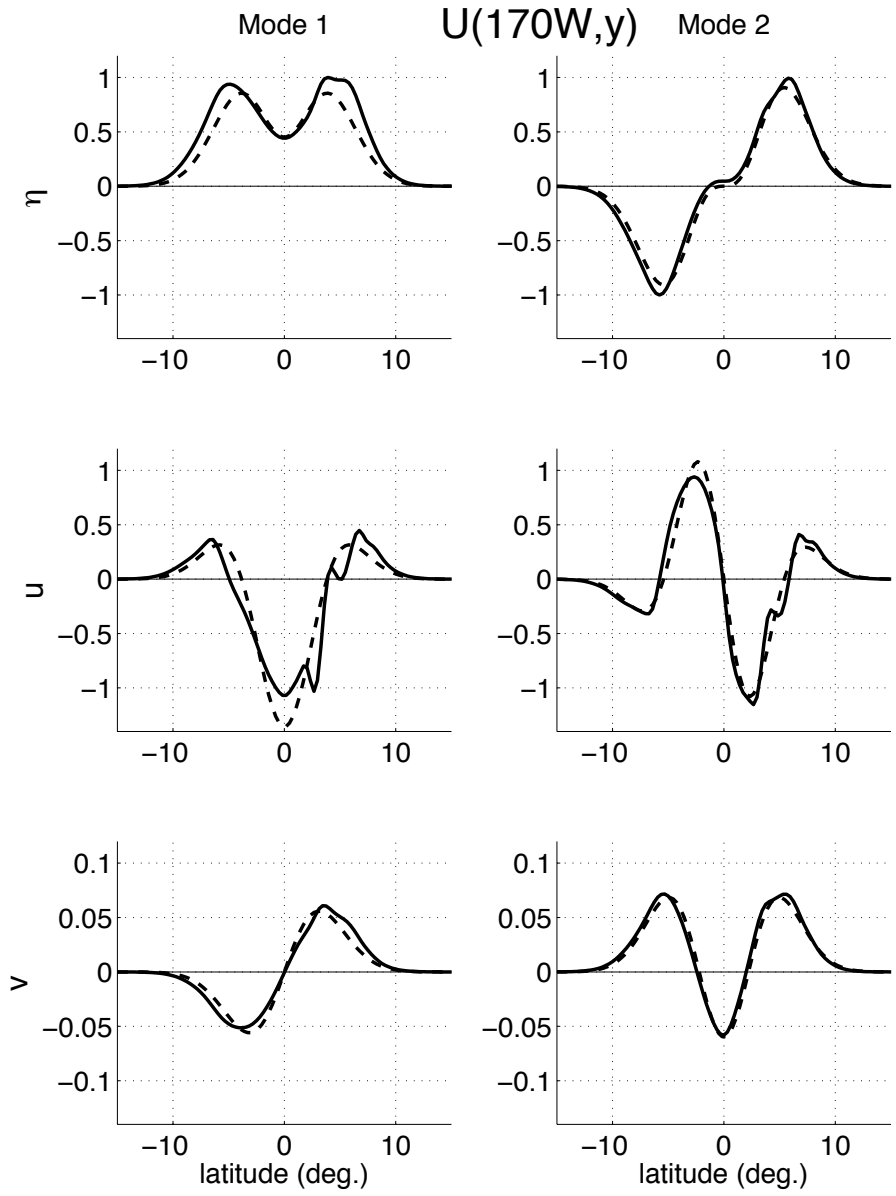

FIG. 4. Long-Rossby wave eigenfunctions at the annual period: meridional modes 1 (left column) and 2 (right column). Solid curves represent numerical solutions of shallow-water equations linearized about the currents at $170W$. Dashed curves are classical solutions for no mean flow.

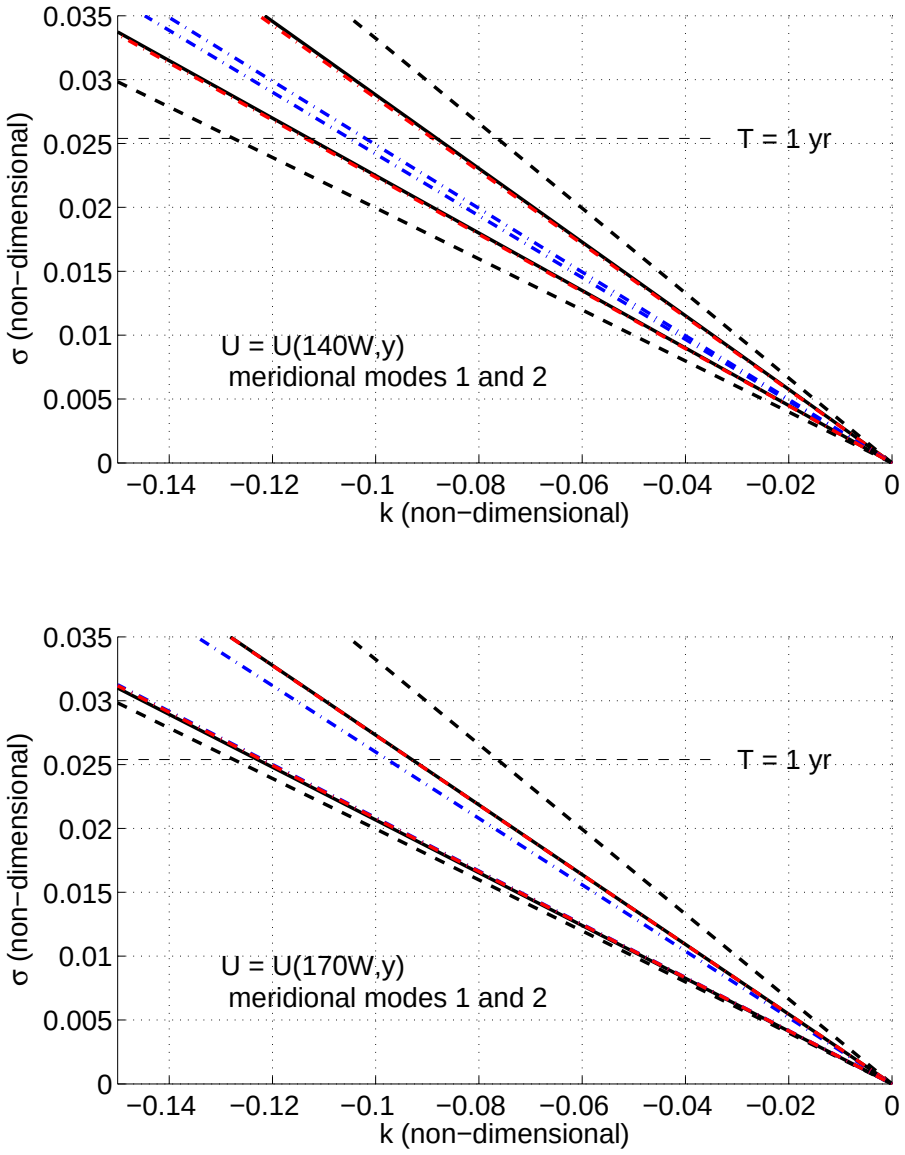

FIG. 5. Long Rossby wave dispersion relations for meridional modes 1 and 2. Upper panel: $U = U(140W, y)$ solutions. Lower panel: $U = U(170W, y)$ solutions. Dashed black curves: $O(1)$ (Hermite) solutions, dashed blue curves: $O(\epsilon)$ solutions, dashed red curves: $O(\epsilon^2)$ solutions. Numerical solutions are represented by black solid curves.

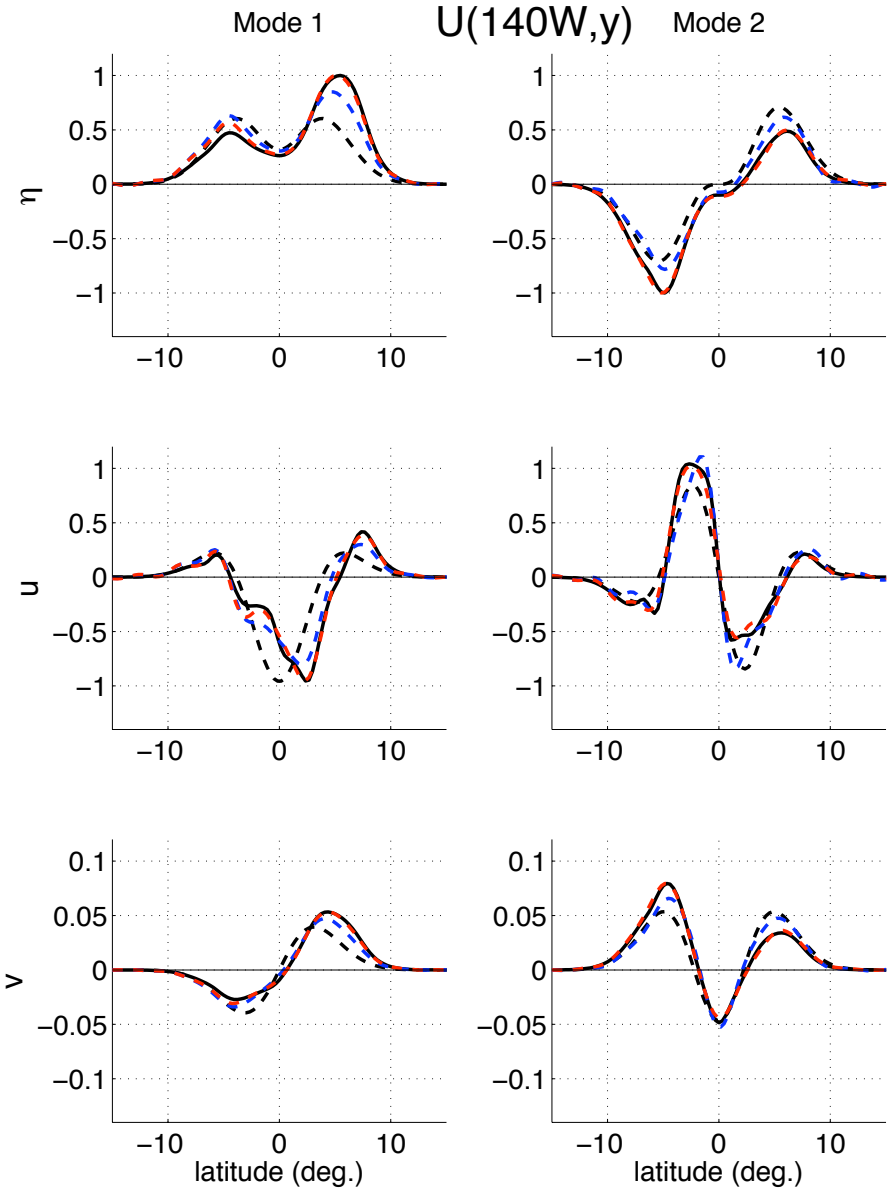

FIG. 6. Long Rossby wave η, u and v eigenfunctions for $U = U(140W, y)$: meridional modes 1 and 2 at the annual period. Twenty Hermite Rossby modes are included in the corrections. Dashed black curves: $O(1)$ (Hermite) solutions, dashed blue curves: $O(\epsilon)$ solutions, dashed red curves: $O(\epsilon^2)$ solutions. Numerical solutions are represented by black solid curves.

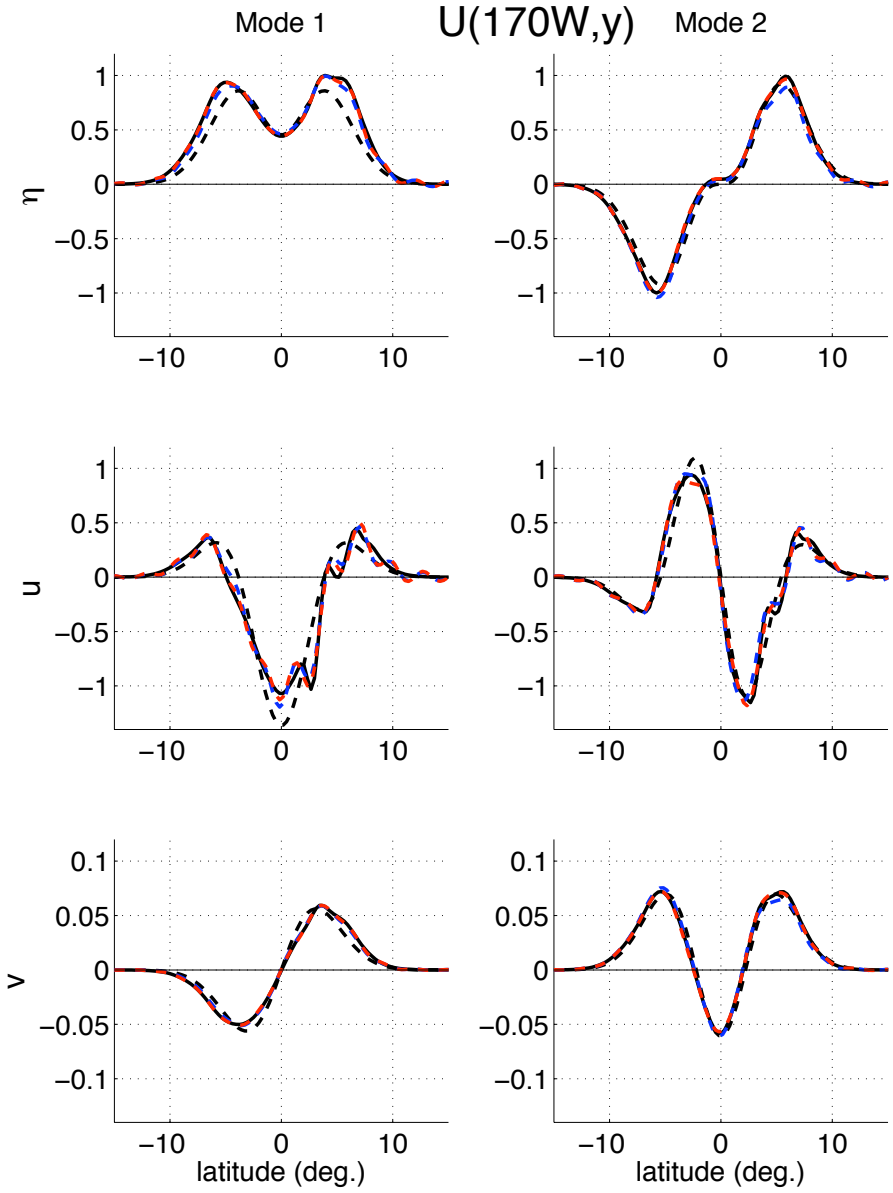

FIG. 7. Long Rossby wave η, u and v eigenfunctions for $U = U(170W, y)$: meridional modes 1 and 2 at the annual period. Thirty Hermite Rossby modes are included in the corrections. Dashed black curves: $O(1)$ (Hermite) solutions, dashed blue curves: $O(\epsilon)$ solutions, dashed red curves: $O(\epsilon^2)$ solutions. Numerical solutions are represented by black solid curves.

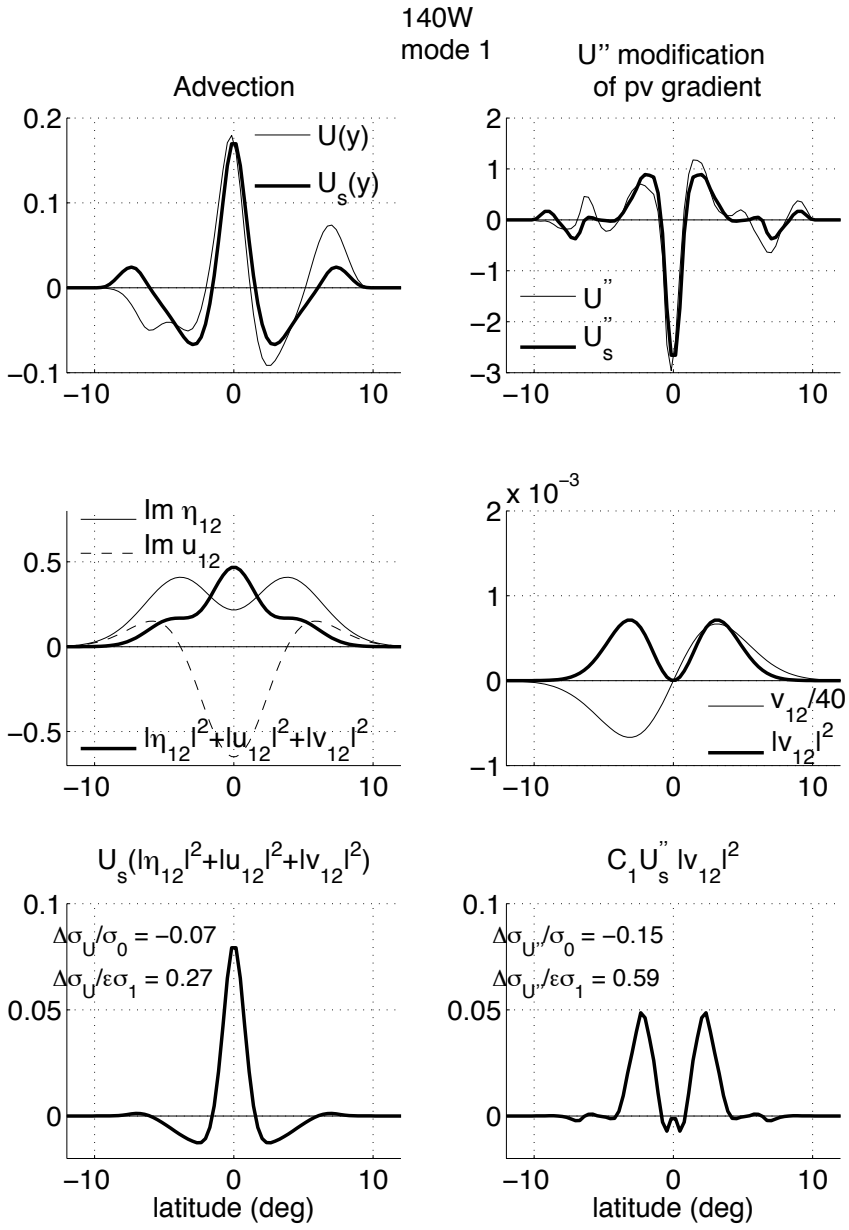

FIG. 8. Effects of advection (left column) and U'' (right column) on mode-1 phase speed at $140W$. Top row: meridional profile of mean-current feature (thin curve) and its symmetric part (thick curve). Middle row: squared amplitude of the part of the Hermite wave field affected by the current feature above it. Bottom row: projection of mean current feature onto relevant wave-field structure (product of thick curves in top and middle rows). $C_m = -(\sigma_{m2}/k)\int_{-\infty}^{\infty}|u_{m2}|^2dy/\int_{-\infty}^{\infty}|v_{m2}|^2dy$, $\Delta\sigma/\sigma_0$ is the relative change in frequency and $\Delta\sigma/\epsilon\sigma_1$ is the fractional contribution to the total $O(\epsilon)$ frequency correction.

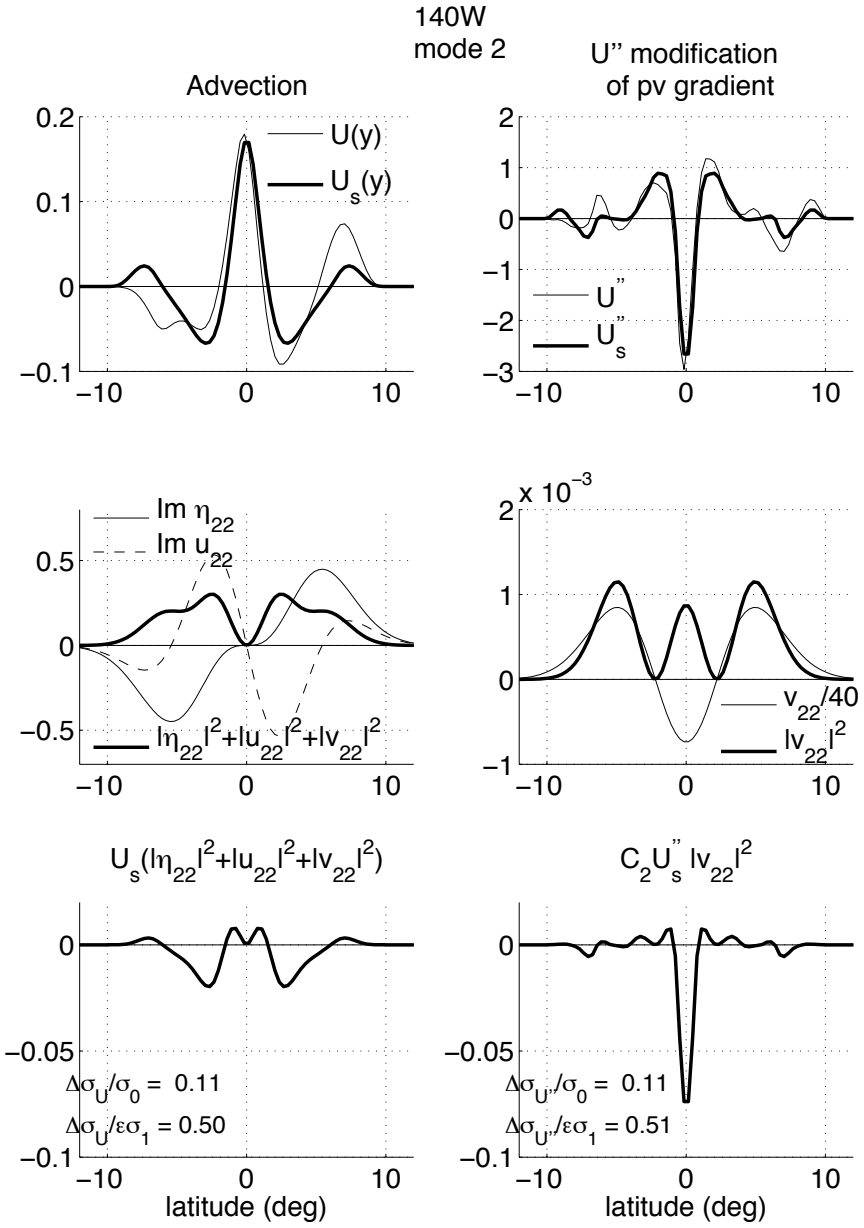

FIG. 9. Effects of advection (left column) and U'' (right column) on mode-2 phase speed at $140W$. Same format as fig. 8.

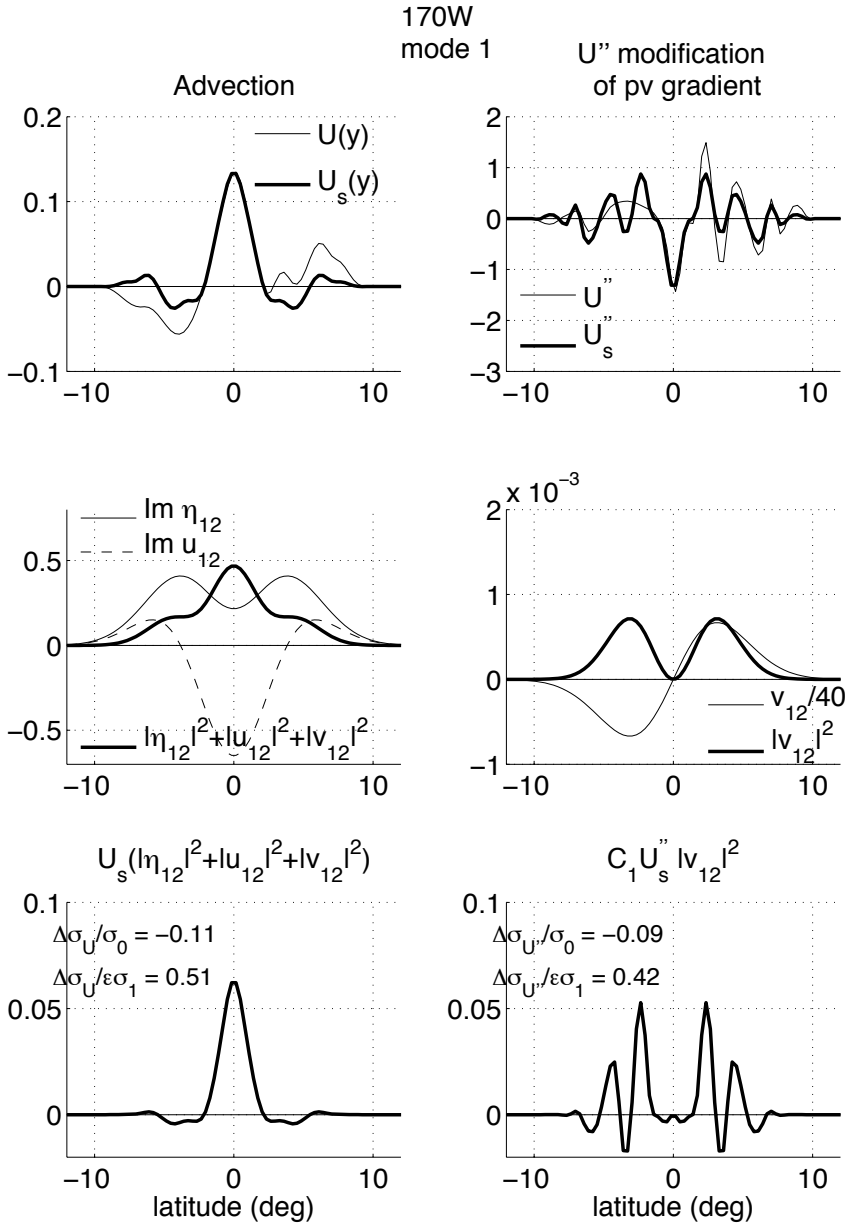

FIG. 10. Effects of advection (left column) and U'' (right column) on mode-1 phase speed at $170W$. Same format as fig. 8.

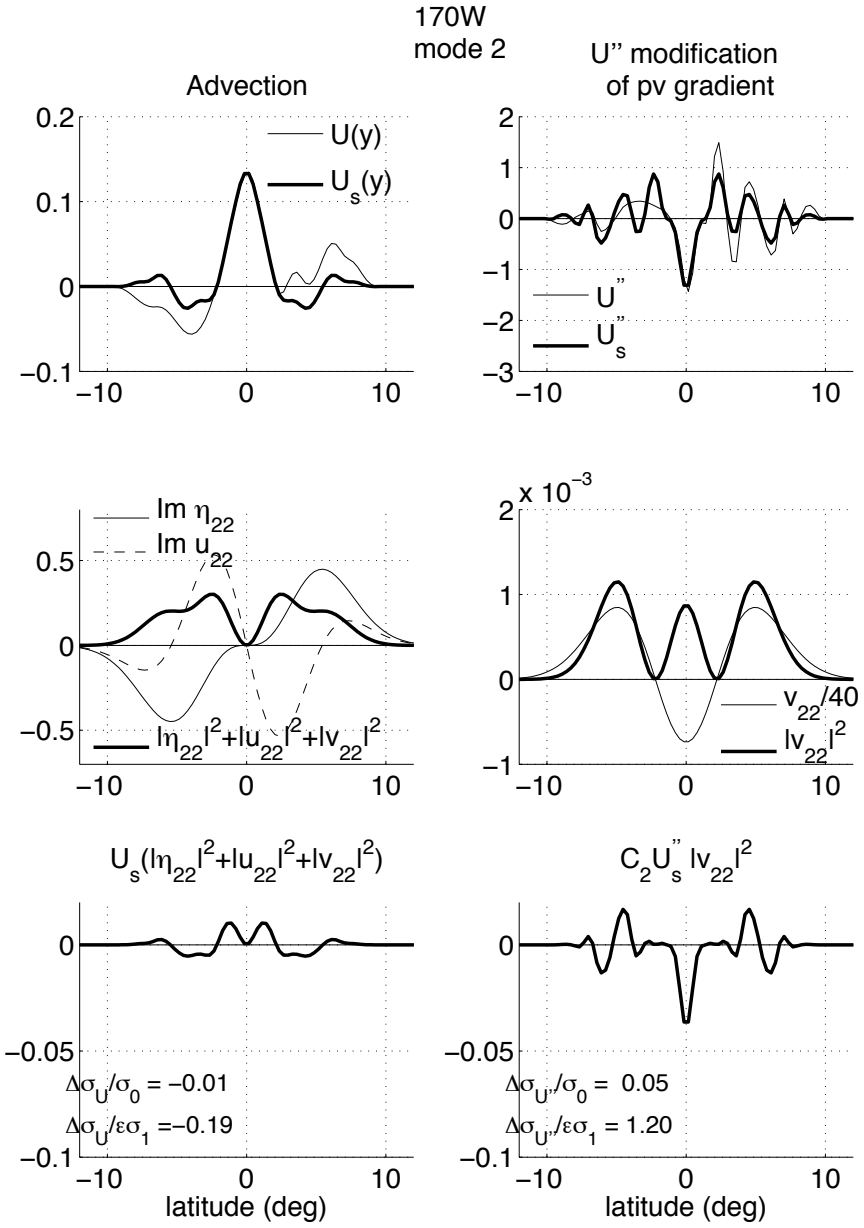

FIG. 11. Effects of advection (left column) and U'' (right column) on mode-2 phase speed at $170W$. Same format as fig. 8.

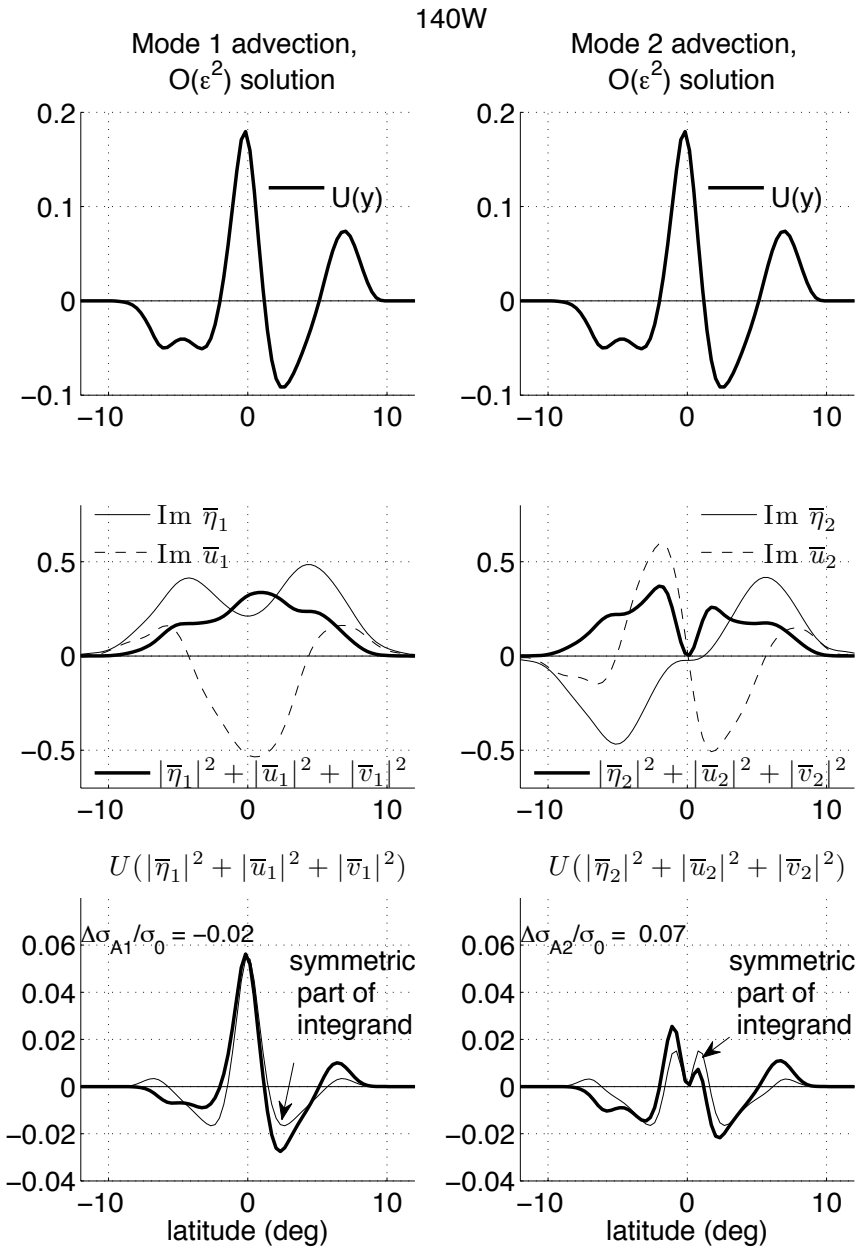

FIG. 12. Advective effects on mode 1(left column) and mode 2 (right column) in the $O(\epsilon^2)$ frequency solutions. Similar format to left columns of figs. 8-11, except that the thick curve in the top panels represents the full U profile (not just the symmetric part). The middle panels display the important parts of the average wave vectors defined by (43), with subscripts indicating the meridional mode number M. The thick curve in the bottom panel is the integrand of (46) and $\Delta\sigma_{AM}/\sigma_0$ is the relative change in phase speed by advection in the $O(\epsilon^2)$ solution of mode M.

List of Tables

	mode #	$\epsilon\sigma_1/\sigma_0$		$\Delta\sigma/\sigma_0$		
			$\widehat{U}$	$-\widehat{U}''$	$-2y\widehat{\delta H}'$	$-y(\widehat{U}'+2y\widehat{\delta H})$
$U(140W,y)$	1	-0.25	-0.07	-0.15	-0.04	$+0.01$
	2	$+0.21$	$+0.11$	$+0.11$	-0.02	$+0.02$
$U(170W,y)$	1	-0.22	-0.11	-0.09	-0.01	-0.00
	2	$+0.044$	-0.009	$+0.053$	-0.003	$+0.005$

TABLE 1. $O(\epsilon)$ frequency corrections for meridional modes 1 and 2 by $U(140W,y)$ (upper section) and $U(170W,y)$ (lower section). The first column is the meridional mode number, the second shows the relative frequency change at $O(\epsilon)$, and the following columns give the separate contributions to σ_1 of the terms on the right-hand side of (26). Each column header designates the feature of the mean current that appears in the integrand of the term. Note that the effective β term has been separated into its two components: $-\hat{U}''$ and $-2y\,\delta\hat{H}'$. In general, the frequency changes are dominated by the advection ($\hat{U}$) and/or the pv gradient modification due to the curvature of the mean current ($\hat{U}''$).